https://doi.org/10.5194/egusphere-2026-5025
Preprint. Discussion started: 16 September 2026

Integrated satellite monitoring and field validation of the periodically outbursting glacier-dammed lake Nedre Demmevatnet, Norway

Ronja Lappe[1], Ursula Enzenhofer[1,5], Pascal E. Egli[1], Yongmei Gong[1,3], Liss M. Andreassen[2], Andreas Kääb[4], Martina Calovi[1]

[1]Department of Geography and Social Anthropology, Norwegian University of Science and Technology, Trondheim, 7049 Norway
[2]Section for Glaciers, Ice and Snow, Norwegian Water Resources and Energy Directorate (NVE), Oslo, 0301 Norway
[3]IPCC WGI TSU, Université Paris Saclay, 91190 Gif sur Yvette, France
[4]Department of Geosciences, University of Oslo, Oslo, 0371 Norway
[5]Department of Geology, University Centre in Svalbard (UNIS), Longyearbyen, 9171 Norway

Correspondence to: Ronja Lappe (ronja.lappe@ntnu.no)

Abstract.

Glacial Lake Outburst Floods (GLOFs) present a significant hazard in warming alpine environments, but detailed, sub-seasonal studies of ice-dammed glacier lakes remain rare due to data scarcity. To overcome this challenge, we reconstruct nearly a decade (2016-2025) of drainage timings, outburst volumes, lake levels, and automated, machine learning-based sub-seasonal lake refilling cycles at the ice-dammed lake Nedre Demmevatnet (southwestern Norway), dammed by the glacier Rembesdalskåka, an outlet glacier of the Hardangerjøkulen ice cap. By integrating publicly available satellite and meteorological datasets, we evaluate remote sensing capabilities and establish an error budget for tracking a small and highly dynamic water body. We validate our spaceborne findings using field measurements, including water-level loggers, time-lapse cameras, a local automatic weather station, and high-resolution UAV photogrammetry, complemented by PlanetScope imagery. Combining Sentinel-1 and Sentinel-2 imagery, we constrain GLOF drainage windows to ± 2 days. Lake volume sensitivity tests revealed that while satellite outline errors are minor (2.6–4.2 %), using the static regional digital elevation model ArcticDEM (2014) causes a 25.5 % volume underestimation compared to our 2022 UAV bathymetry due to rapid ice-dam retreat and lakebed erosion. Crucially, the time gap between the last cloud-free satellite image and the GLOF introduces a relative daily volume underestimation of 1.7 %, which scales up significantly during cloudy periods. Our validated multi-sensor remote sensing approach enables valuable glaciological insights, revealing that GLOF timings shifted earlier by an average of 10 days, alongside shortened refilling periods over the past 9 years. Between 2016 and 2022, pre-GLOF lake levels reached 1236–1239 m a.s.l., closely matching the theoretical hydrostatic flotation threshold. In contrast, the 2023 event drained at approximately 1224 m a.s.l. – more than 10 m below this threshold – following a shortened melt period indicated by fewer positive degree days, possibly due to opening of subglacial channels through melt. Finally, we synthesize the workflow developed and tested on our case study into an operational framework that facilitates transferability to other rapidly changing ice-dammed lakes.

https://doi.org/10.5194/egusphere-2026-5025
Preprint. Discussion started: 16 September 2026

1 Introduction

Glacier lake outburst floods (GLOFs), also referred to as *jøkulhlaups,* are sudden and often catastrophic releases of meltwater stored in lakes impounded by glaciers, moraines, or bedrock barriers (Benn and Evans, 2014). GLOFs are high-magnitude events that can cause severe impacts to downstream communities, infrastructure, and ecosystems (Taylor et al., 2023). While moraine-dammed lakes typically generate a single, large-volume outburst, ice-dammed lakes generally hold smaller water volumes but can outburst repeatedly, posing new threats to downstream areas each time (Carrivick and Tweed, 2016). Driven by ongoing atmospheric warming, the number and area of glacial lakes have increased globally since the 1990s (Shugar et al., 2020), which led to debates regarding related shifts in GLOF frequency and magnitude (Harrison et al., 2018; Taylor et al., 2023; Veh et al., 2019, 2023; Zheng et al., 2021). While some modelling predicts that GLOF risk could nearly triple (Zhang et al., 2024; Zheng et al., 2021), global historical inventories show no clear increase in overall GLOF frequency in response to glacial retreat yet (Harrison et al., 2018; Veh et al., 2019). For ice-dammed lakes specifically, accelerating deglaciation was in fact observed to have thinned and destabilized ice dams, which led to decreasing peak flood magnitudes and shifting drainage timing earlier into the season (Rick et al., 2023; Veh et al., 2023, 2025), making the impact of climate change on GLOFs an open and debated research topic.

Assessing how these systems respond to climate change requires a process-based understanding of their drainage mechanisms. The triggering and subsequent drainage of ice-dammed GLOF events is highly complex, varying with among other factors local weather, climate conditions, ice conditions (such as temperature), and not least glacier and lake geometry. An often-described outburst mechanism is the flotation of the ice dam, which occurs when the lake's hydrostatic pressure exceeds the ice overburden pressure (Thorarinsson, 1939). This uplift at the ice-bed interface can initiate drainage and subsequently drive subglacial channel enlargement (Nye, 1976; Tweed and Russell, 1999). Consequently, predicting flotation events requires detailed knowledge of both lake levels and ice-dam thickness. Yet, ice-dammed lakes have also been observed to drain before reaching the flotation threshold, either driven by viscoplastic deformation (Carrivick et al., 2017), siphoning (Carrivick et al., 2017; Tweed and Russell, 1999), or a continuous connection to the glacier's drainage system (Jenson et al., 2022). Since these processes are highly dynamic and vary between individual basins, capturing the exact onset, timing and magnitude of GLOFs remains a major challenge (Jenson et al., 2022; Zheng et al., 2021).

Given the difficult accessibility of high-alpine environments, the application of remote sensing has become fundamental to tracking glacial lake dynamics and outburst floods (Aggarwal et al., 2016). While in-situ measurements remain essential for calibration and validation (Bazai et al., 2021), they are often time-consuming, costly, and spatially and temporally discontinuous (Kääb et al., 2016). Remote sensing data can bridge this gap by transferring local findings to larger scales. Recent advances in the availability and resolution of satellite imagery have therefore significantly increased our understanding of GLOF occurrence (Amin et al., 2020; Emmer et al., 2022; Wangchuk et al., 2022). Current methodologies primarily utilize multispectral indices, such as the Normalized Difference Water Index (NDWI) (McFeeters, 1996), derived from high-resolution optical archives like Landsat and Sentinel-2 to track lake evolution. To mitigate the challenges of frequent cloud

https://doi.org/10.5194/egusphere-2026-5025
Preprint. Discussion started: 16 September 2026

cover in mountainous terrain, Synthetic Aperture Radar (SAR) data has been increasingly employed, which offers all-weather, day-and-night imaging capabilities (Tom et al., 2025). However, the effective use of SAR data is limited by geometric distortions, such as layover and shadowing in steep terrain as well as misclassification of water with other smooth surfaces such as wet snow or sand (Lodigiani et al., 2026; Strozzi et al., 2012; Wangchuk et al., 2019). Glacial lake detection methods range from manual digitization (Wang et al., 2015; Zhang et al., 2015) and semi-automatic classification (Bazilova and Kääb, 2022; Bolch et al., 2008) to fully-automated, cloud-based fusions of optical and SAR imagery (Wangchuk and Bolch, 2020). Despite these advances, automated detection is still challenged by mountain shadows, turbidity, and ice cover (Abderhalden et al., 2024; Lappe and Andreassen, 2026; Wangchuk and Bolch, 2020), though quality is improving through the application of machine learning and artificial intelligence (Tom et al., 2025; Zhang et al., 2024).

Most remote sensing analysis in the field still focuses on the static detection of medium to large glacial lakes (Nie et al., 2013; Rawlins et al., 2026; Shugar et al., 2020), whereas small glacial lakes are often overlooked in global inventories despite their potential for devasting downstream impacts (Abderhalden et al., 2024; Narama et al., 2018; Zhang et al., 2024). Furthermore, detailed sub-seasonal studies of ice-dammed lakes remain rare and are mainly focused on Iceland, North America, and the European Alps (Veh et al., 2019, 2023). At the same time, an urgent need for local, trigger-focused analysis and lake evolution studies has been recognized as a major research gap in the field (Emmer et al., 2022). This also includes reconstructing GLOF volumes and resolving meteorological conditions prior to outbursts (Carrivick and Tweed, 2016). A general lack of in-situ measurements of GLOF lakes, such as high-resolution bathymetry and continuous lake-level records, further complicates validation of remote sensing observations (Zhang et al., 2024, 2026). To overcome this data scarcity, previous studies used empirical volume-area relationships to estimate GLOF volumes, finding that lake area and volume are generally well-correlated (Cook and Quincey, 2015; Huggel et al., 2004). However, while these models help identifying GLOF volumes on large scales, they lack the site-specific accuracy required for individual case studies (Zhang et al., 2024).

In Norway, GLOFs are almost exclusively associated with ice-dammed lakes (Nagy and Andreassen, 2019a), historically threatening downstream infrastructure and agricultural communities (Liestøl, 1956). In addition to multiple nationwide glacial lake inventories (e.g. Andreassen et al., 2022; Lappe and Andreassen, 2026; Nagy and Andreassen, 2019b), the Norwegian Water Resources and Energy Directorate (NVE) has used Sentinel-1 and -2 images to inspect and monitor approximately 40 GLOF locations over the last years (Andreassen et al., 2021). However, targeted scientific investigation of individual Norwegian GLOF lakes remain rare (exceptions include: Abderhalden et al., 2024; Elvehøy et al., 1997; Engeset et al., 2005). The most significant historical and contemporary GLOF events in Norway occurred at the glacier-dammed lake Nedre Demmevatnet. Documented outbursts from this lake date back to 1736, with catastrophic events in the late 19th century releasing up to 35 million m^3 of water into the Simadalen valley within a single day (Liestøl, 1956). These repeated disasters led to some of the earliest engineering-based GLOF mitigation measures, including the construction of an initial rock drainage tunnel in 1899 at 1293 m a.s.l., followed by a second tunnel 54 meters below in 1938, designed to artificially restrict the lake's maximum volume (Elvehøy et al., 1997, 2002; Jackson and Ragulina, 2014). Although these interventions successfully provided 76 years without outbursts, the extensive contemporary thinning and retreat of the Rembesdalskåka glacier dam has

https://doi.org/10.5194/egusphere-2026-5025
Preprint. Discussion started: 16 September 2026

caused the tunnels to be ineffective, triggering a new era of annual drainage events since August 2014 (Kjøllmoen et al., 2025). The hazardous potential, however, has significantly decreased compared to the early 20th century due to reduced lake volumes and the establishment of the downstream hydropower reservoir Rembesdalsvatnet, that captures the outburst discharges (Kjøllmoen et al., 2022). Thus, Nedre Demmevatnet presents an ideal natural laboratory for investigating outbursts of ice-dammed lakes, offering relatively easy accessibility compared to remote sites in Alaska, Canada, or High Mountain Asia.

Our study addresses the identified technical, regional, and process-based research gaps by reconstructing GLOF timing, volume and level as well as sub-seasonal lake evolution, at Nedre Demmevatnet between 2016 and 2025 using openly available satellite and meteorological data, validated against field observations. Building on this, we evaluate the potential transferability of our monitoring approach to data-scarce regions and discuss the implications of our findings for understanding local GLOF mechanisms. This study aims to answer the following three research questions (RQ):

- **RQ1**: How precisely can openly available satellite data analysis constrain GLOF timing, volume and level as well as sub-seasonal lake evolution for a small ice-dammed lake and which error sources dominate?
- **RQ2**: What would it take to transfer the presented monitoring framework to regions lacking in-situ observations?
- **RQ3**: What do the reconstructed filling and drainage dynamics together with local weather data reveal about the underlying drainage mechanisms?

2 Study area

This study focuses on the ice-dammed glacial lake Nedre Demmevatnet close to the terminus of Rembesdalskåka, a western outlet glacier of the Hardangerjøkulen ice cap in southern Norway (61°30'N, 7°30'E), located at 1237 m a.s.l. (Fig. 1). Hardangerjøkulen is Norway's sixth-largest glacier, covering an area of 64.1 km² (map year of 2019; Andreassen et al., 2022). In recent years, Nedre Demmevatnet has covered an area of approximately 0.14 km^2 in its full stage (Kjøllmoen et al., 2025). Rembesdalskåka is located at the weather divide between eastern and western Norway characterised by a cold, humid maritime alpine climate with mean annual temperatures ranging between 0 and -6°, annual precipitation between 1400 and 1800 mm and an annual average of 200-350 days with more than 25 cm snow for the reference climate period 1991-2020 (Tveito, 2021). Mass balance measurements at Hardangerjøkulen show a long-term negative trend since the late 1990s, consistent with regional warming and increased melt (Kjøllmoen et al., 2022, 2025). The area of the ice cap has been greatly reduced since its Little Ice Age maximum extent (Weber et al., 2020), resulting in parts now being detached from the main glacier and a 9% reduction in overall area from 2003 to 2019 (Andreassen, 2022; Andreassen et al., 2022).

https://doi.org/10.5194/egusphere-2026-5025
Preprint. Discussion started: 16 September 2026

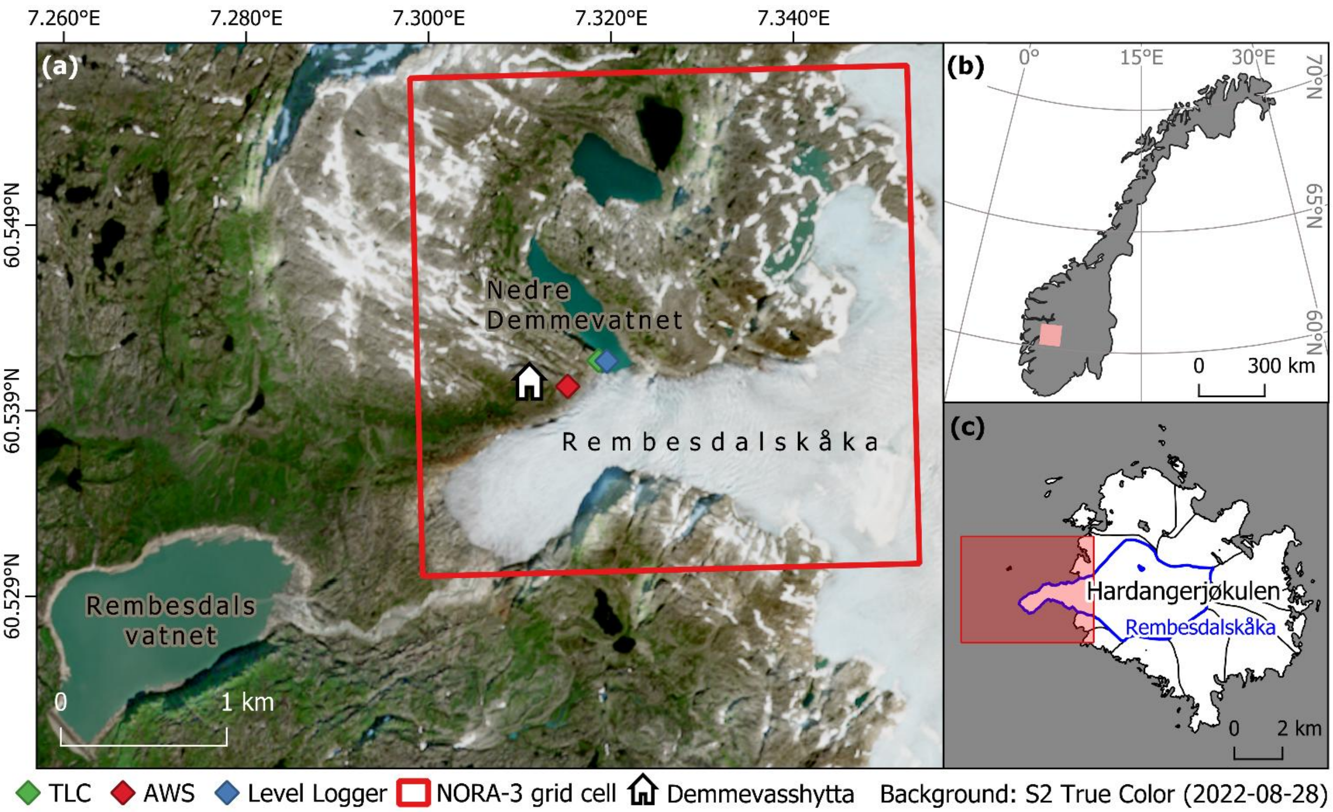

Figure 1: Overview map of the study area: b) Norway, c) Hardangerjøkulen ice cap highlighting the basin of Rembesdalskåka, a) Location of ice-dammed lake Nedre Demmevatnet and the downstream hydropower reservoir Rembesdalsvatnet, as well as the locations of the in-situ measurements: Time-lapse camera (TLC), Automatic Weather station (AWS) and water level logger. The red bounding box represents the NORA-3 reanalysis weather data grid cell extent.

3 Data & Methods

3.1 Remote sensing and weather data

The monitoring of GLOFs at Nedre Demmevatnet presented in this study relied on a multi-sensor approach, integrating only publicly available, large-scale datasets from satellite platforms, digital elevation models (DEM) and re-analysis weather data (Table 1).

3.1.1 Satellite images

We used freely available Sentinel-2 multispectral satellite imagery from the European Space Agency's (ESA) Copernicus programme. This constellation, which originally consisted of two identical satellites (2A and 2B) launched in 2015 and 2017, now also includes Sentinel-2C since 2024 (ESA, 2026). Sentinel-2 offers a 5-day temporal resolution and captures 13 spectral bands at spatial resolutions ranging from 10-60 m (Drusch et al., 2012). While our study primarily relied on atmospherically

https://doi.org/10.5194/egusphere-2026-5025
Preprint. Discussion started: 16 September 2026

corrected Surface Reflectance (SR) products, Top of Atmosphere (TOA) imagery was occasionally used in cases where SR imagery was not available (Gascon et al., 2017).

To mitigate the limitations of cloud cover in manual GLOF detection, the optical observations were supplemented with Sentinel-1 Synthetic Aperture Radar (SAR) data, providing consistent all-weather monitoring since 2014. Specifically, we employed dual-polarized Ground Range Detected (GRD) products acquired in the C-band Interferometric Wide (IW) swath mode. The GRD preprocessing of the GRD SAR data includes thermal noise removal, radiometric calibration as well as terrain correction based on ASTER DEM, providing a consistent spatial resolution of 10 m (Torres et al., 2012).

Table 1: Overview of publicly available datasets used in this study.

Data	Date	Resolution	Description	Provider/ Reference
Harmonized Sentinel-2 SR and TOA (S2)	2016-2025	10-60 m	12 bands, atmospherically corrected (SR)	ESA/ Copernicus (ESA, 2025b)
Sentinel-1 SAR GRD (S1)	2016-2025	10 m	VV-polarized, IW instrument mode, Ground Range Detected, calibrated, ortho-corrected	ESA/ Copernicus (ESA, 2025a)
PlanetScope/ RapidEye (PS)	2016-2025	2.4 – 4.8 m	5 bands, atmospherically corrected, radiometrically balanced, geometrically aligned, restricted access	ESA/ Planet (Planet, 2023)
Copernicus GLO-30 DEM	2011-2015	30 m	Based on Tandem-X radar mission	(ESA and Airbus, 2022)
ArcticDEM Strip	2014	2 m	Based on satellite optical stereo photogrammetry	PGC (Polar Geospatial Center) (Porter et al., 2022)
Norwegian national elevation model (NDH-DTM)	2020	min. 1 m	Based on laser scan and photogrammetry data acquired between 2010-2021	(Kartverket, 2025)
Norwegian reanalysis weather data (NORA3)	2016-2025	3x3 km	daily temporal resolution, Norwegian hindcast data based on meteorological modelling forced by ERA5 and running from surface-level weather data	MET.no (Norwegian Meteorological Institute) (Furevik and Haakenstad, 2025)
MET Norway weather station at Finsevatn (SN25830)	2016-2025	Point (60.594° N, 7.527° E)	Real-time and archived weather data, 10 min temporal resolution, located at 1,210 m a.s.l.	MET.no (Norwegian Meteorological Institute) (MET Norway, 2025)

To validate results from publicly available satellite images, very high-resolution (VHR) multispectral PlanetScope imagery was selectively employed. These images are acquired by a fleet of approximately 200 "Dove" nanosatellites, providing near-daily global coverage at a spatial resolution of 3 m in 8 spectral bands since 2014 (Planet, 2023). For this study, we utilized the PlanetScope SR product, which is orthorectified and atmospherically corrected to ensure spectral consistency with other satellite missions. Limited access to the images was possible through the Basic Education and Research license, which offers a free download quota of 3000 km^2 per month.

https://doi.org/10.5194/egusphere-2026-5025
Preprint. Discussion started: 16 September 2026

3.1.2 Digital elevation models

For the satellite-based GLOF volume reconstructions, a 2 m ArcticDEM strip from 2014-09-04 was used as it represents the Nedre Demmevatnet lakebed after lake drainage, exposing its full bathymetry. The ArcticDEM, produced by the National Geospatial-Intelligence Agency (NG) and the National Science Foundation (NSF), provides high-resolution DEM generated from Worldview satellite optical stereo imagery via photogrammetry. For this study, a single strip was used rather than the mosaic to retain maximum detail and an accurate time stamp. Strip DEMs represent the overlapping portions of WorldView stereopair swaths and typically cover ~17×115 km (Porter et al., 2022).

To support the automated water classification, the Copernicus GLO-30 DEM was selected as it captures the lake in its full stage. This ensures that the classifier does not erroneously omit pixels within the basin. The global product derived from the TandDEM-X interferometric radar mission between 2011 and 2015, provides a 30 m spatial resolution. Post-processing includes flattening of water bodies and ensuring consistent flow of rivers (ESA and Airbus, 2022).

High-resolution topographic data for Hardangerjøkulen were obtained from Kartverket's Høydedata NDH dataset from 2020 (Kartverket, 2025). The data is derived from point clouds based on airborne laser scanning and aerial image matching between 2010 and 2020, yielding a 1 m spatial resolution Digital Terrain Model (DTM) with a vertical accuracy of ~0.1–1 m. The dataset was used as reference for co-registration.

3.1.3 Re-analysis weather data

Norwegian NORA3 hindcast data, aggregated on a daily timescale, was used to provide continuous weather data for the ablation season (May – October) during the period 2016 to 2025. NORA3 data represents an integration of globally available ERA5 re-analysis weather data with surface weather observations using the weather model HARMONIE-AROME (Bengtsson et al., 2017; Müller et al., 2017; Seity et al., 2011). It has a high spatial resolution of 3 x 3 km, providing a better representation of local topography and a significantly improving performance in modelling 2-m air temperature and daily precipitation compared to ERA5 data (Haakenstad et al., 2021; Haakenstad and Breivik, 2022).

For validation, the NORA3 data from the cell covering the tongue of Rembesdalskåka and Nedre Demmevatnet (Fig. 1) was compared to our own local Automatic Weather Station (AWS) at Demmevasshytta (AWS Demmevass) (see Sect. 3.2.4), as well as to the closest MET Norway station, AWS Finsevatn (Table 1) for summer 2023, when continuous 2-m air temperature was available from AWS Demmevass. The AWS Finsevatn (SN25830, 1210 m.a.s.l.; MET Norway, 2025), is located on the NE side of Hardangerjøkulen at a horizontal distance of 13 km from the ice dam and nearly at the same elevation above sea level as the glacier tongue.

3.2 Field data

To validate the satellite-derived observations and provide high-resolution ground truth, we collected in-situ field measurements at Nedre Demmevatnet between 2022 and 2025. These include topographic data from Unmanned Aerial Vehicle (UAV)

https://doi.org/10.5194/egusphere-2026-5025
Preprint. Discussion started: 16 September 2026

photogrammetry, barometric records from pressure loggers, visual confirmation from time-lapse cameras and data from an AWS. The integration of these field-based observations allows for robust assessment of the drainage and refilling events identified in the satellite time series.

3.2.1 UAV DEM

UAV surveys were conducted on 25 September 2022 using a DJI Phantom 4 Pro V2.0 over the completely drained lakebed of Nedre Demmevatnet to reconstruct its bathymetry. Two single-grid, nadir-view flights were executed at a constant altitude with 80 % overlap. To ensure high spatial accuracy, ground control points (GCPs) were distributed across the lakebed, and their coordinates acquired using two Leica dGNSS receivers with real-time kinematic (RTK) positioning in a base-rover configuration. The base station data was post-processed in static mode using local network RINEX data to refine the rover's stop-and-go RTK measurements. The acquired aerial images were processed in Agisoft Metashape following a standard photogrammetry workflow, which included image alignment, sparse 3D point cloud generation, and GCP-based geometric optimization (Over et al., 2021). A final densification algorithm was applied to interpolate the point cloud into high-resolution products. The resulting DEM and orthophoto mosaic were exported with Ground Sampling Distances (GSDs) of 0.04 and 0.02 m, respectively.

3.2.2 Water level logger

To monitor lake level changes, submerged hydrostatic water pressure loggers were deployed between 2022 and 2024 (Fig. 1). Each Spring, the water level logger was attached to a steel wire drilled into bedrock and lowered as far as possible into the filling lakebed, weighed with a rock. It was recovered once the lake had emptied in late summer. A barometric pressure logger was installed nearby to correct atmospheric pressure. A mini-diver from van Essen Instruments was used in the first year and Solinst level loggers in subsequent years. Because the loggers could not safely be anchored at the absolute lakebed (due to the possibility of bed erosion processes), measurements were used to calculate relative water level variations. Hydrostatic pressure readings were corrected for atmospheric variations using the barometric data. The water column height above the loggers (h, in meters) was converted using standard hydrostatic principles:

$$h = \frac{P_{abs} - P_{atm}}{pg} \tag{1},$$

where P_{abs} is the absolute pressure recorded at the submerged logger, P_{atm} is the atmospheric pressure, p the density of the water (approximated at 1000 kg/ m^3) and g is the gravitational acceleration (9.81 m/s^2).

3.2.3 Time-lapse camera

Time-lapse cameras were deployed during the spring field seasons in 2023 and 2024 for monitoring both the lake refilling and drainage and recovered after each GLOF event. A Brinno BCC2000 time-lapse camera was used in 2023, while Technaxx TX-164 Full HD cameras were installed in subsequent years. The cameras were configured for time-lapse photography with a 10-

https://doi.org/10.5194/egusphere-2026-5025
Preprint. Discussion started: 16 September 2026

minute interval and mounted on the orographically right-hand side of the lake at a 100 m distance from the ice dam (Fig. 1). The mounting was drilled into an overhanging rock, and the camera was placed on a telescope arm.

3.2.4 Automatic weather station

The HOBO MicroRx2100 AWS Demmevass, was installed approximately 80 m near-vertically above the glacier tongue of Rembesdalskåka, on the orographically right-hand side of the glacier on a bedrock outcrop near the DNT cabin Demmevasshytta (Fig. 1) during the summer months of 2023-2025 (April-August). Sensors for measuring air temperature, relative humidity, wind speed, wind direction, barometric pressure, and shortwave radiation were installed. Data was collected only during the summer months relevant for snow- and ice melt, lake filling, and subsequent outburst floods, and to avoid damages to the weather station from winter storms and snow loading. Unfortunately, several sensors malfunctioned during certain time periods, especially during large parts of summer 2025. The data measured by this AWS was used to assess the representativeness of NORA3 reanalysis data (Haakenstad et al., 2021; Haakenstad and Breivik, 2022).

3.3 Satellite data analysis and field validation

Our methodological approach for monitoring GLOF cycles at Nedre Demmevatnet with publicly available data combines manual GLOF identification and volume reconstruction with an automated classification of lake refilling (Fig. 2). To test its reliability, the remote sensing observations were verified with in-situ field measurements, official GLOF records and commercial VHR satellite imagery.

3.3.1 Identification of GLOF timings

To determine the timing of past GLOFs, satellite scenes closest to known drainage events were identified manually. Sentinel-1 and Sentinel-2 images were screened using the Copernicus Browser (Sentinel-Hub, 2025) and cross-referenced with dates from NVE's GLOF inventory (Kjøllmoen et al., 2025; NVE, 2026b). The combined date was estimated by intersecting the Sentinel-1 and Sentinel-2 detection intervals, defined by the last pre-event and first post-event acquisitions. The resulting overlap window was used as the feasible drainage period, while its midpoint was taken as the best GLOF estimate. The uncertainty was calculated as ± half the window width. All scenes with visible water area were included in this analysis. The manual identification approach serves as a best-case benchmark for assessing the feasibility of detecting GLOFs with openly available satellite imagery.

3.3.2 Lake volume and lake level reconstruction

For GLOF lake level and volume estimations, pre-drainage Sentinel-2 image dates were selected, where the area over the lake was completely cloud-free. Within the cloud-computing platform Google Earth Engine (GEE) (Gorelick et al., 2017), the

https://doi.org/10.5194/egusphere-2026-5025
Preprint. Discussion started: 16 September 2026

images were automatically co-registered to a reference Sentinel-2 median composite and the Normalized Difference Water Index (NDWI) (McFeeters, 1996) was calculated prior to downloading.

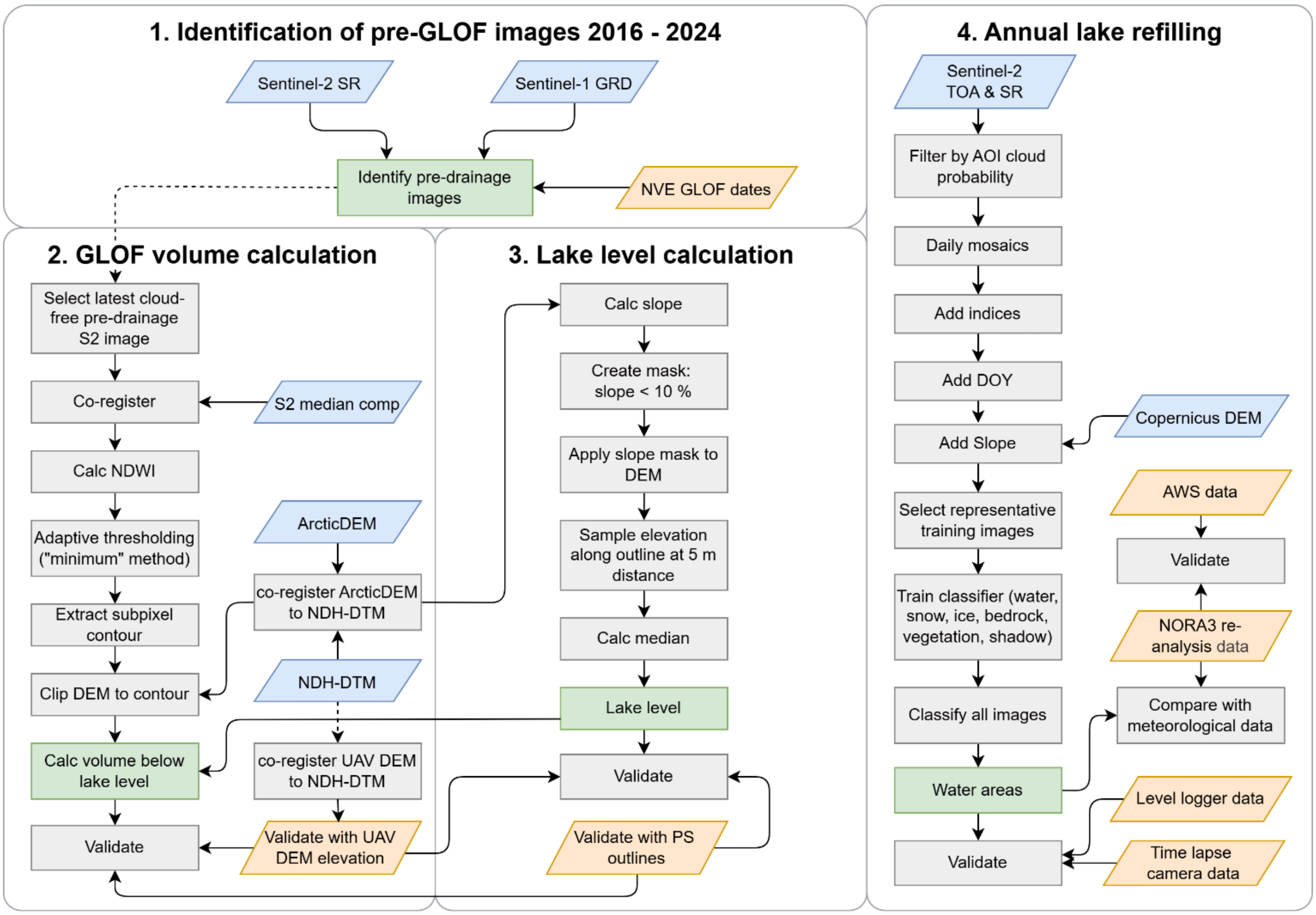

Figure 2: Schematic workflow showing the different components of the satellite data analysis to (1) manually identify GLOF timings, (2) reconstruct GLOF volumes, (3) translate pre-drainage lake outlines into lake levels, (4) automatically derive lake refilling and compare to meteorological data. S2 refers to Sentinel-2, PS to PlanetScope, NDH-DTM to the Norwegian elevation model (Table 1).

To determine the boundary between land and water within each NDWI image, several histogram-based thresholding methods implemented in the Python library "skimage" (Van Der Walt et al., 2014) were compared. Among these, the "minimum"-method – which converts a grey-level image into a binary image by smoothing the image histogram until two dominant maxima remain and selecting the minimum value between them as the threshold (Glasbey, 1993) – performed best for our case, particularly in delineating water from ice. Since automatic thresholding ideally requires a bimodal histogram distribution (Ng et al., 2013), each image was clipped to a generalized buffered polygon of "Nedre Demmevatnet" to ensure a similar distribution of land and water pixels. A sub-pixel outline was then extracted by applying the "skimage.measure.find_contour" function, which is based on a marching squares algorithm and uses the derived threshold to interpolate between neighbouring pixel values and delineate a precise land-water boundary (Van Der Walt et al., 2014).

https://doi.org/10.5194/egusphere-2026-5025
Preprint. Discussion started: 16 September 2026

Both the ArcticDEM and the UAV DEM were co-registered to the reference 2020 NDM-DTM (Table 1) over stable terrain following the method of Nuth and Kääb (2011) using the "xdem" Python package (xDEM contributors, 2026). Outliers were excluded using vector masks, and the target datasets were reprojected to the reference grid prior to alignment while preserving native grid resolutions. Co-registration performance was evaluated over stable terrain, improving the normalized median absolute deviation (NMAD) of elevation differences from 0.50 m before co-registration to 0.28 after alignment.

Subsequently, a slope layer was derived in addition to surface elevation. To retrieve one representative lake level from the lake outline, elevation and slope values were sampled at 10 m distance along the outline and then filtered by a slope threshold of 10° as elevation can more reliably be retrieved in flat terrain. The median of the filtered elevation values was used as the representative lake level. The DEM was then clipped to each lake outline, and the volume calculated below the extracted lake level as follows:

$$Volume = Area_{Pixel} \times \sum (H_{level} - h_i) \quad (2),$$

where $Area_{Pixel}$ is the 2D area of a single pixel, H_{level} the reference elevation (the extracted lake level) and h_i the elevation of pixel i in the DEM, where $h_i < H_{level}$.

Validation with UAV DEM and VHR satellite data

To evaluate the impact of the chosen DEM on the lake level and volume reconstructions, we repeated the same analyses using the UAV DEM instead of the satellite-based ArcticDEM and compared the differences. To assess the accuracy of the automatically derived Sentinel-2 lake outlines, we selected pre-drainage dates for which both Sentinel-2 and VHS PlanetScope imagery was available. The PlanetScope images were co-registered to the corresponding Sentinel-2 scenes using the QGIS Georeferencer tool (QGIS project, 2026) by selecting 10 evenly distributed GCPs for each PlanetScope image. Shifts between the mapped and the references outlines were then assessed along shore-perpendicular transects by quantifying the distance between the intersection points of both outlines with the transects. The median value was used to represent the lake outline error. To quantify the impact of the Sentinel-2 outline uncertainty on lake level and volume, we repeated the analyses with the PlanetScope reference outlines and compared the results.

Finally, to account for the impact of the time delta between the latest cloud-free available Sentinel-2 image and the drainage date, we selected years in which PlanetScope images closer to the drainage date were available, mapped the lake outlines and compared the resulting lake levels and volumes to the respective Sentinel-2 outlines.

3.3.3 Automatic identification of lake refilling

To capture the refilling of Nedre Demmevatnet, we developed an automated classification approach using multi-temporal supervised pixel-based classification. This methodology follows the principles of Satellite Image Time Series (SITS) analysis, which uses the temporal evolution of spectral signatures to improve classification robustness in dynamic environments (Simoes et al., 2021). The image processing was carried out in Google Earth Engine (GEE) for the years 2016-2025. The primary data source consisted of the Sentinel-2 image collection, utilizing the TOA collection for images prior to 2018 and the SR collection

https://doi.org/10.5194/egusphere-2026-5025
Preprint. Discussion started: 16 September 2026

for images from 2018 onwards to ensure long-term consistency. To maintain high data quality while maximizing the number of available observations, a multi-stage cloud filtering process was applied. Images with more than 80 % scene-wide cloud cover were initially excluded. The Sentinel-2 collections were then paired with the "S2_cloud_probability" dataset (EO Research, 2020; GEE, 2025). To identify images that were cloud-free over the lake area and unimpacted by cloud shadows, we calculated cloud probability within a 10 m and a 1,000 m buffer over the lake outline and filtered out images with more than 20 % and 30 % cloud cover in these respective areas.

The remaining observations were then aggregated into daily mosaics to provide a clean, spatially continuous dataset. For each resulting mosaic, a high-dimensional feature stack was generated to improve the separability of water, ice, and mountain shadows. This stack included the original spectral bands 2 (Blue), 3 (Green), 4 (Red), 8 (NIR), 11 (SWIR1), and 12 (SWIR2), alongside several spectral indices, following the standards suggested by Montero et al. (2023): the Normalized Difference Water Index (NDWI) (McFeeters, 1996), Normalized Difference Snow Index (NDSI) (Riggs et al., 1994), Normalized Difference Vegetation Index (NDVI) (Rouse et al., 1974), Normalized Difference Glacier Index (NDGlal) (Keshri et al., 2009) and the Automated Water Extraction Index with Shadows Elimination (AWEIsh) (Feyisa et al., 2014), which are calculated as follows:

$$NDWI = \frac{G-N}{G+N} \tag{3}$$

$$NDSI = \frac{G-S1}{G+S1} \tag{4}$$

$$NDVI = \frac{(N-R)}{N+R} \tag{5}$$

$$NDGlal = \frac{G-R}{G+R} \tag{6}$$

$$AWEIsh = (B + 2.5 * G - 1.5 * (N + S1) - 0.25 * S2) \tag{7}$$

where B is Band 2 (Blue), G Band 3 (Green), R Band 4 (Red), N Band 6 (NIR), $S1$ Band 11 (SWIR1) and S2 Band 12 (SWIR2). Furthermore, a Day of Year (DOY) band was included as a predictor variable. By incorporating DOY, the model learns the seasonal variations in water, snow and ice appearance, a technique that has proven essential in distinguishing land cover across different seasons in machine learning time series applications (Nieto et al., 2021; Račič et al., 2024; Yuan and Lin, 2020). Topographic context was provided by adding a slope band derived from the Copernicus GLO-30 DEM (Table 1), which represents Nedre Demmevatnet in its full stage, ensuring the classifier does not erroneously eliminate water pixels due to high-slope values typically found in empty lake basins.

The classification was performed using a Random Forest model consisting of 500 trees. The model was trained using seven representative images from 2017 (TOA) and 2018 (SR) selected to capture the full range of phenological and atmospheric conditions throughout the year: winter (snow), spring (melt), summer (open water), and autumn (refreeze and long shadows) for both Sentinel-2 datasets. Training data was sampled using a date-specific approach: for each training image, pixels were extracted only from polygons digitized specifically for that acquisition date. This ensured that the spectral signatures in the training dataset matched the ground conditions of the six classes: water, snow, shadow, bedrock, vegetation,

https://doi.org/10.5194/egusphere-2026-5025
Preprint. Discussion started: 16 September 2026

and ice. All pixels within these digitized polygons were sampled and merged into a comprehensive training data set, resulting in 20967 samples. The data was split into a 70 % training and 30 % validation set, to assess the quality of the final classification. Following validation and an assessment of feature importance, this optimized model was applied to the entire 2016-2025 time series to systematically map the lake refilling processes.

Validation with level logger data and time-lapse camera images

In addition to the internal validation of the Random Forest classifier using the validation set, refilling curves were additionally validated against independent field measurements. To verify the timing and duration of specific refilling and drainage events, relative lake-level changes recorded by in-situ level loggers during the 2023 and 2024 melt seasons (see Sect. 3.2.2) were plotted against the satellite-derived lake area changes. Since the logger in 2022 was installed in August, when the lake was already filled, it was only used to validate the timing of the outburst. Furthermore, the refilling curves were cross-checked against time-lapse camera footage from 2023 and 2024 to provide qualitative confirmation of the observed lake dynamics.

3.3.4 Comparison of lake refilling and drainage with weather data

The timing of lake refilling and drainage was compared to local weather station and reanalysis data, as well as calculated degree-day melt, to investigate a possible relationship with local short-term weather conditions. For each summer from 2016 until 2025 degree-day melt and temperature trends before drainage were calculated from Norwegian NORA3 reanalysis data (Table 1). The usefulness of the 3x3 km cell resolution reanalysis data was tested by comparing it to data from AWS Demmevass and AWS Finsevatnet (Table 1). Degree-day melt models, also called temperature index models, are widely used in glaciology to estimate daily melt rates based on air temperature above zero degrees, and a correction factor Degree Day Factor (DDF). Such models are usually adjusted using existing mass balance measurements or new ablation stake measurements to calibrate the Degree Day Factor, indicating how much melt is produced from each degree Celsius above zero degrees (Braithwaite and Raper, 2007). Here, the chosen degree-day factor was 5.5 mm w.e. per °C per day, and the melt threshold temperature was set to 0.0°C according to values for glaciers in Southern Norway derived in Laumann and Reeh (1993).

https://doi.org/10.5194/egusphere-2026-5025
Preprint. Discussion started: 16 September 2026

4 Results

4.1 Identification of GLOF timings

Across all events, the combined Sentinel-1/2 approach yielded the lowest temporal ambiguity, with a mean uncertainty of ±2.0 days (Fig. 3), compared to ±7.0 days for Sentinel-2 alone and ±2.3 days for only Sentinel-1 (Table S1, Fig. S1). Sentinel-1 data was not available in useful proximity to the outburst time for the 2022 and 2023 events. This could be related to the failure of one satellite in the constellation (Sentinel-1B) in December 2021 which significantly decreased image availability until the launch of Sentinel-1C in December 2024 (ESA, 2024). No satellite-based detection was possible for 2017 when the GLOF was late on 27 October and 2025 when the GLOF was very early on 25 April as the lake was ice and snow covered on available cloud-free images.

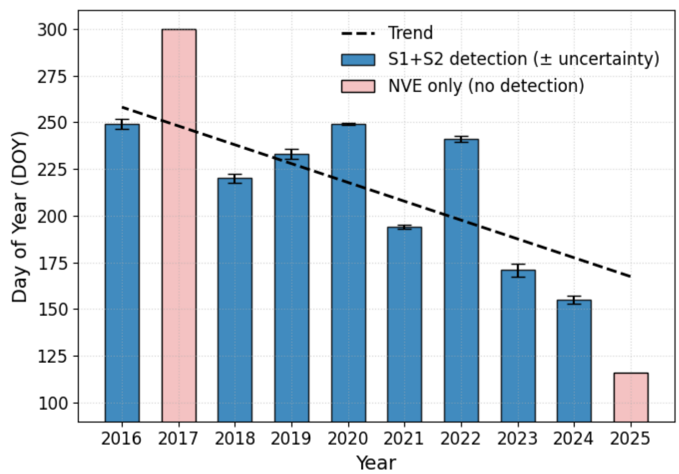

Figure 3: GLOF dates between 2016 and 2025, showing the capability of combining Sentinel-1 and 2 data to detect GLOF events with a certainty of ±2 days, except for the years with very late (2017) and very early drainages (2025), where drainage dates could only be retrieved from the NVE inventory (NVE, 2024).

A temporal trend toward earlier drainage is evident over the study period, with a linear shift of -10 days per year (R^2=0.54, p=0.04), indicating a moderate but statically significant shift in GLOF timing (Fig. 3).

4.2 Lake level and lake volume calculation

Lake levels, derived from the Sentinel-2 pre-GLOF lake outlines and the ArcticDEM, range between 1205 and 1237 m a.s.l., with a mean standard deviation of 8.7 m across the 2016 – 2024 period (Fig. 4a). This range is logical, as the diversion tunnel built in 1938 at 1239 m a.s.l. restricts the maximum lake level (Elvehøy et al., 1997). We excluded the year 2025 as no cloud-free satellite images with recognizable water area were available prior to drainage (see Sect. 4.1). The volumes derived from the Sentinel-2-based lake levels and the ArcticDEM fluctuate between 0.05 million (M) m^3 in 2024 and 1.62 M m^3 (Fig. 4b). When comparing the lake level and volume calculations based on the ArcticDEM to calculations based on the field-based UAV DEM (Sect. 3.2.1), we see slightly lower lake levels derived from the UAV DEM for most years resulting in a mean difference of -0.22 m (-0.01 %) compared to the mean lake level (Fig. 4c). The volume calculations, however, show proportionally larger differences with systematically higher values derived from the UAV DEM with a mean difference of -0.27 M m^3 translating to a mean volume difference of -25.5 % (Fig. 4d). This discrepancy is mainly attributable to the difference in acquisition time between the two DEMs, with the ArcticDEM acquired in 2014 and the UAV DEM in 2022. Subtracting the ArcticDEM from the UAV DEM (Fig. 5) reveals clear elevation differences in the area of the ice dam, which has retreated by approximately 50 m. This retreat has expanded the lake's bathymetry, providing more space for the lake to

https://doi.org/10.5194/egusphere-2026-5025
Preprint. Discussion started: 16 September 2026

fill. The observed lowering of the lakebed close to the 2014 ice-dam position is attributable to a combination of bed erosion and ice melt (Fig. 5).

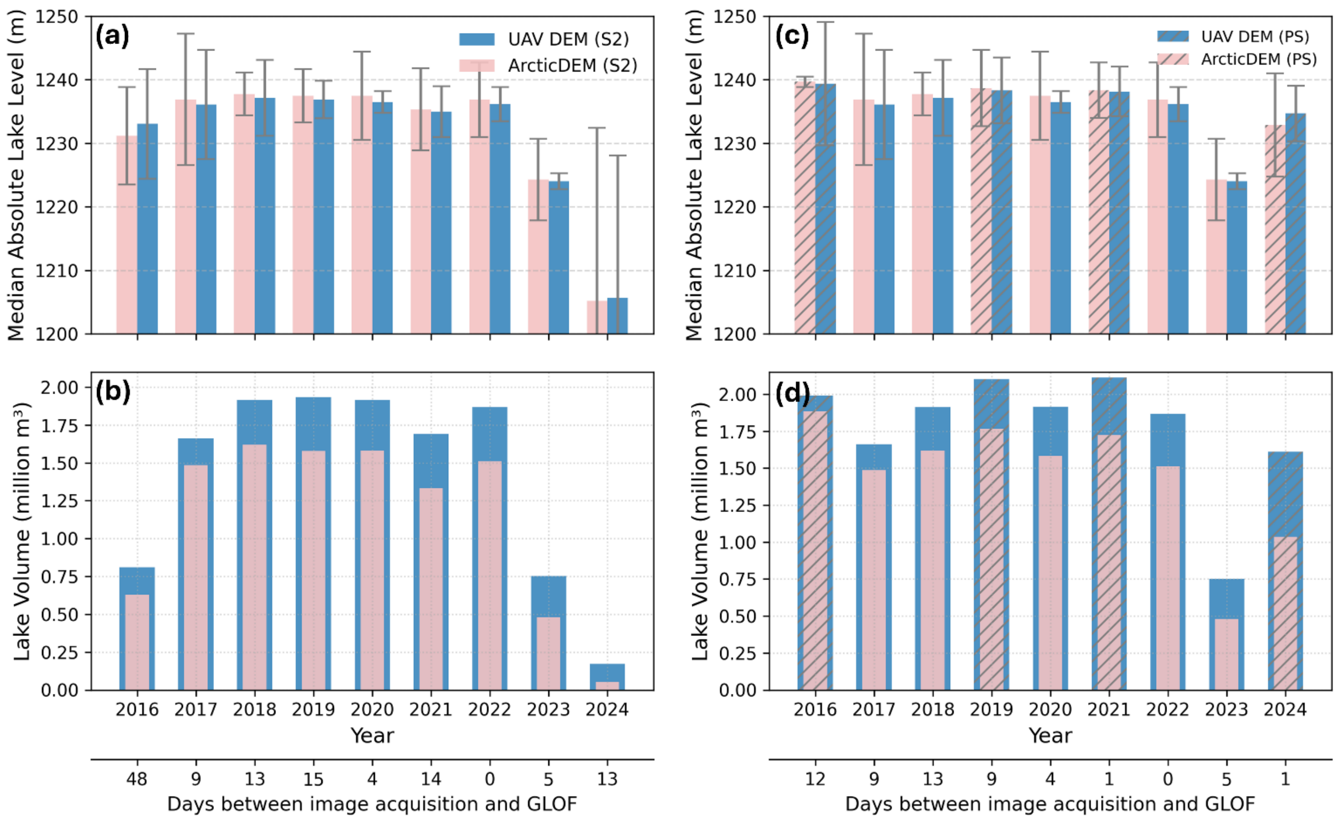

Figure 4: Reconstructed pre-GLOF absolute lake levels (a, c) and corresponding lake volumes (b, d) for Nedre Demmevatnet (2016-2024), comparing the satellite-based ArcticDEM (pink bars) to the field-based UAV DEM (blue bars). Left panels (a, b) show estimates derived using lake outlines mapped from Sentinel-2 (S2) imagery. Right panels (c, d) show estimates updated using VHR PlanetScope (PS) imagery. Grey diagonal hatching in (c) and (d) highlight years, where a PS image was available closer to the actual GLOF date compared to S2. The second x-axes in the bottom show the number of days between the latest available cloud-free satellite image and the GLOF date. Error bars in (a) and (c) represent the standard deviation of elevation values sampled along the lake outlines on terrain with slope < 10°.

A significant additional source of uncertainty in GLOF volume reconstruction is related to the temporal gap between the latest available cloud-free Sentinel-2 image prior to drainage and the actual drainage event, ranging from zero days in 2022 to 48 days in 2016 (Fig. 4). To quantify the impact of this error, we calculated volumes based on PlanetScope imagery that was available closer to the drainage date and calculated the average daily volume increase (Table 2). Based on this comparison, the median daily volume increase was 0.03 M m^3 using the ArcticDEM as well as the UAV DEM, though these rates varied considerably between years. Notably, 2024 exhibited the highest daily volume increase with 0.12 – 0.18 M m^3, which coincides with an early-season drainage event and a supposedly steep refilling curve, whereas other years remained consistent at approximately 0.02 – 0.03 M m^3. When compared to the median PlanetScope-corrected UAV-based lake volume (Fig. 4d), this corresponds to a relative daily volume increase of 1.7 % per day. The respective median daily lake level increase was

https://doi.org/10.5194/egusphere-2026-5025
Preprint. Discussion started: 16 September 2026

calculated at 0.23 – 0.24 m when using the ArcticDEM and UAV DEM, respectively. Compared to the median PlanetScope-corrected UAV-based lake level (Fig. 4c), this translates to a relative lake level underestimation of 0.02 % for every day that lies between the latest full-lake image acquisition and the drainage date. While volumes and lake levels prior to drainages seemed to haven been generally similar between 2016 and 2024, there is a notable decline in 2023 with a significantly lower lake level and volume, despite showing an average time gap of 5 days between the latest satellite image and the drainage event.

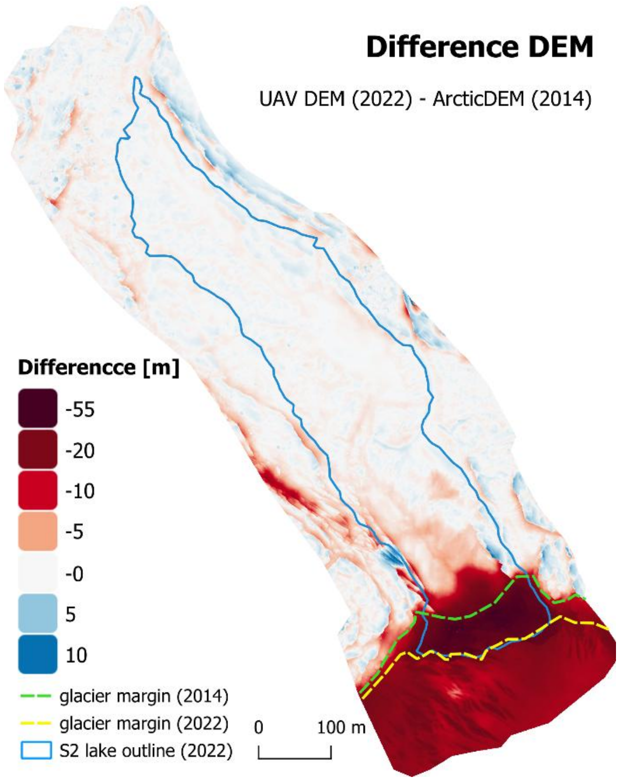

Figure 5: Difference between the UAV DEM (2022) and ArcticDEM (2014) in the area of Nedre Demmevatnet.

Table 2: Volume error induced through the time delta between the latest available cloud-free Sentinel-2 (S2) image and the GLOF event. Showing the difference in calculated lake volume when using PlanetScope (PS) lake outlines closer to the GLOF date, comparing the ArcticDEM with the UAV DEM for volume calculations.

Year	GLOF date	S2 date	PS date	S2 time delta [days]	PS time delta [days]	Vol. change/ day [M m^3] (Arctic DEM)	Vol. change/ day [M m^3] (UAV DEM)	Level change/ day [m] (ArcticDEM)	Level change/ day [m] (UAV DEM)
2016	6 Sep	20 Jul	25 Aug	48	12	0.03	0.03	0.23	0.18
2019	24 Aug	9 Aug	15 Aug	15	9	0.03	0.03	0.20	0.24
2021	13 Jul	24 Jun	12 Jul	19	1	0.02	0.02	0.17	0.18
2024	4 Jun	22 May	31 May	13	4	0.16	0.18	3.60	3.44
2024	4 Jun	22 May	3 Jun	13	1	0.12	0.14	2.70	2.58
					Median:	**0.03**	**0.03**	**0.23**	**0.24**

To address another potential source of error, we calculated the impact of the Sentinel-2 outline accuracy on lake level and volume calculations (Table 3). When compared to the values derived from VHR PlanetScope imagery from the same date, the automatic Sentinel-2 outlines achieved a median accuracy of 4.6 m with a standard deviation of 3.8 m, which lies below the 10 m-sensor resolution of Sentinel-2 imagery. Table 3 shows the impact of the Sentinel-2 outline uncertainty on lake level and

https://doi.org/10.5194/egusphere-2026-5025
Preprint. Discussion started: 16 September 2026

volume calculations, which varies depending on the degree of the shift and the choice of the DEM. The largest differences were recorded in 2022, where also the median outline shift was highest. The mean lake level difference between the Sentinel-2 and PlanetScope outlines amounts to -0.25 m when using the ArcticDEM and -0.57 m with the UAV DEM. The related volume error is -0.03 M m^3 with the ArcticDEM and -0.09 M m^3 with the UAV DEM, respectively.

The relative impact of the outline uncertainty on the lake level averages to -0.02 % for the ArcticDEM and -0.05 % for the UAV DEM and is much smaller compared to the relative impact on the volume calculations with an average of -2.6 % for the ArcticDEM and -4.2 % for the UAV DEM (Fig. 6). Hence, the Sentinel-2 outlines seem to slightly underestimate both the lake level as well as the lake volumes on average.

Table 3: Sentinel-2 (S2) outline uncertainty when compared to manually digitized outlines from PlanetScope imagery (PS) of the same day along shore-perpendicular transects (Median shift) and its impact on lake level and volume calculations using the ArcticDEM and UAV DEM.

Year	Median shift [m]	Median std [m]	Level diff. (S2-PS) Arctic [m]	Vol. diff. (S2-PS) Arctic [M m^3]	Level diff. (S2-PS) UAV [m]	Vol. diff. (S2-PS) UAV [M m^3]
2020	4.27	3.04	0.23	0.01	-0.62	-0.1
2021	3.05	2.96	0.40	0.04	0.42	0.03
2022	7.08	4.02	-1.24	-0.17	-1.94	-0.27
2023	4.13	5.11	-0.42	-0.02	-0.14	-0.01
AVG	**4.63**	**3.78**	**-0.25**	**-0.03**	**-0.57**	**-0.09**

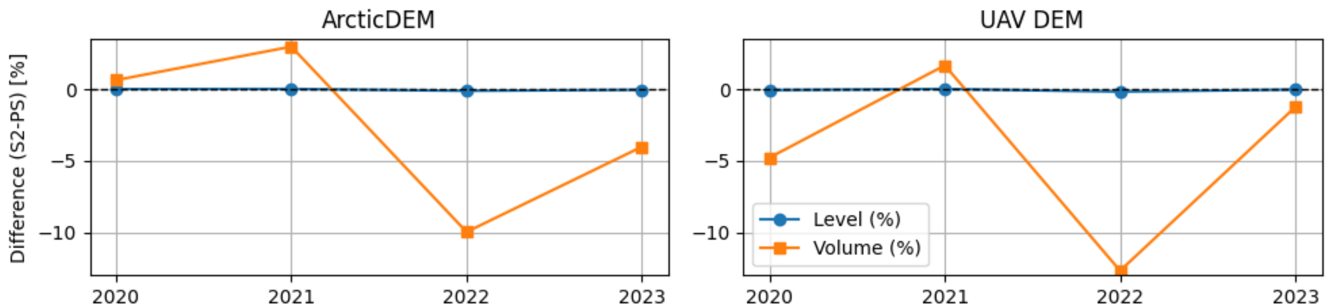

Figure 6: Relative impact of Sentinel-2 outline uncertainty on lake level and lake volume calculations when using the ArcticDEM and UAV DEM.

https://doi.org/10.5194/egusphere-2026-5025
Preprint. Discussion started: 16 September 2026

4.3 Automatic identification of lake refilling

Snow and ice classification dominate the images early in the season as seen in the exemplary classification results for the 2018 time series (Fig. 7). The refilling and emptying of the lake are well depicted through the growing extent of classified water followed by a sudden shift to bedrock post-drainage (3 Sep). Notably, floating lake ice chunks - visible on e.g. 26 May and 8 Jun (Fig. 7) – are categorized as ice rather than water. This is expected to lead to a slight underestimation of the total water area early in the season, a common challenge in alpine water classification (Lappe and Andreassen, 2025; Wangchuk and Bolch, 2020).

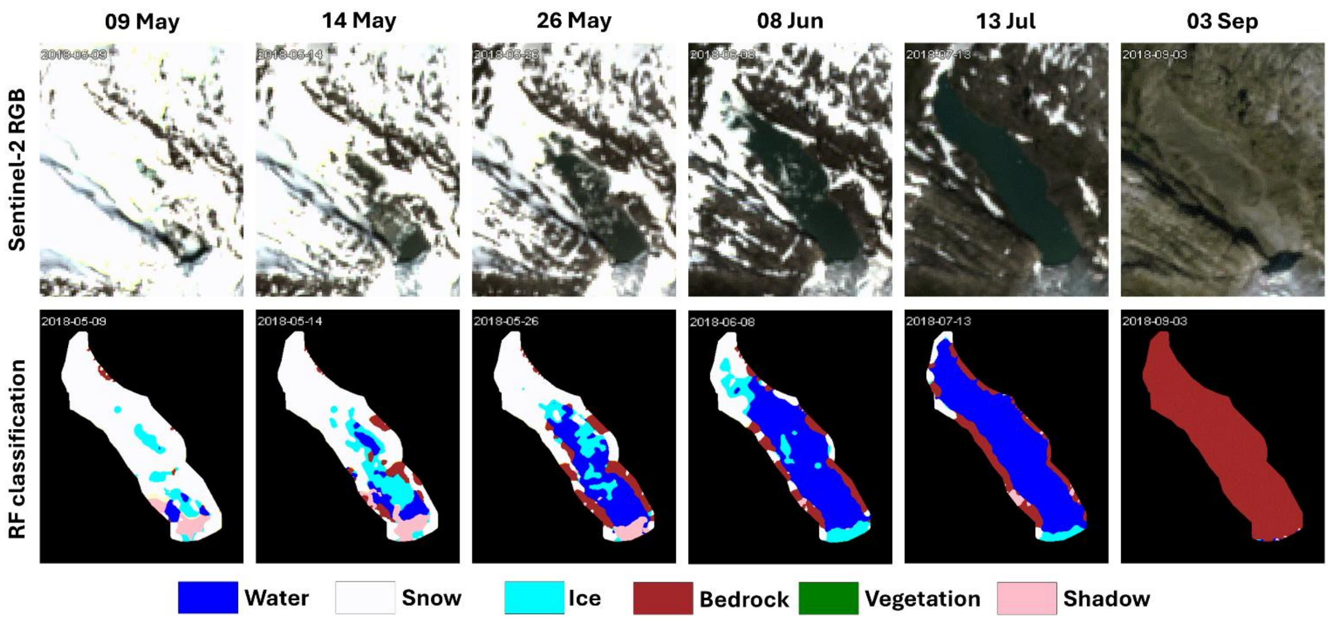

Figure 7: Example lake refilling time-series for 2018 using Random Forest water classification.

While the random forest model yielded an internal Overall Accuracy of 99.7 % (F1-score: 0.997) (Fig. S2), these high metrics are heavily influenced by spatial autocorrelation due to the standard train/ validation split of the training data set, which is a commonly recognized issue in machine learning-based remote sensing (Abriha et al., 2023). Consequently, these accuracy values represent an optimistic, upper-bound validation measure rather than true performance. Visual inspection of the classified outputs (Fig. 7) suggests a higher degree of confusion, particularly between the classes 'shadow' and 'water', as well as 'snow' and 'ice'. A more reliable validation of the classifier's performance is demonstrated through independent cross-checks with field observations at the end of this section (Fig. 10).

The feature importance (Fig. 8) reveals that topography and temporality are the primary drivers of the model performance, with slope (13.7 %) and DOY (11.3 %) being the most important predictors. Given the steep terrain surrounding Nedre Demmevatnet, the high ranking of slope is expected, as it prevents the model from misclassifying terrain shadows as water. The high importance of DOY in the confusion matrix shows the relevance of providing seasonal context to the data to reliably

https://doi.org/10.5194/egusphere-2026-5025
Preprint. Discussion started: 16 September 2026

classify water throughout the seasons. By integrating time of year, the model better recognizes the periods when snow, ice and water are physically likely to be present.

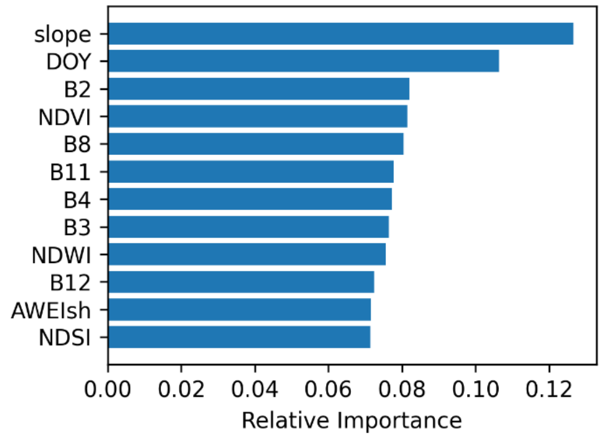

Figure 8: Feature importance for Random Forest classification.

The lake area time series classifications for the years 2016-2025 (Fig. 9) consistently depict a water area increase throughout the summer seasons with a sudden drop prior to or at the time of the reported GLOFs in almost every year with the exception of 2025, where the drainage happened too early in the season to be detectable on available Sentinel-2 imagery (see Sect. 4.1). No large water area detections outside of the melt season or after drainage were recorded, which supports the general robustness of the classifier. The onset of the lake refilling was usually recorded between mid-May and end of July, showing continuously rising lake areas until the time of the drainage with occasional fluctuations (e.g. Fig. 9 – 2017).

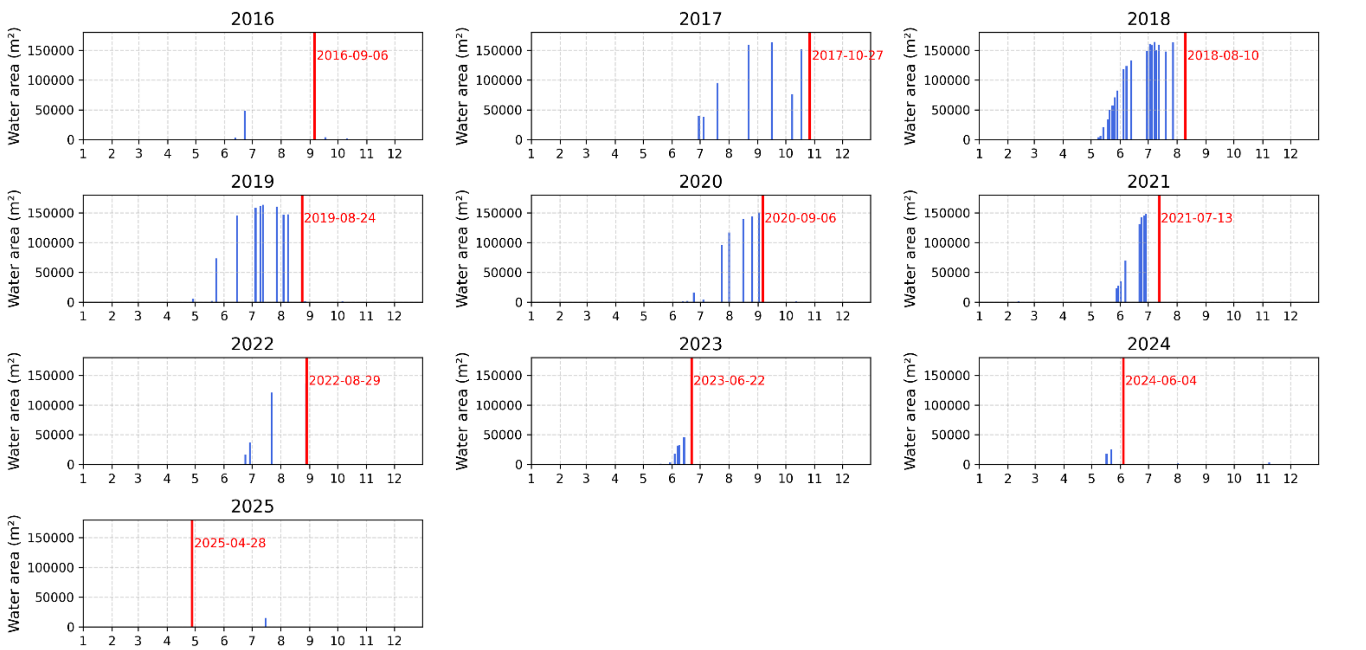

Figure 9: Sentinel-2 based lake refiling time-series between 2016-2025 showing classified water area in each acquisition (blue bars) and the drainage timing from the NVE GLOF inventory (red bar).

The density of the time series differs largely between the years with most available cloud-free acquisitions during the refilling period in 2018 (19 images) and least available acquisitions in 2016 and 2025 (2 and 3 images, respectively) (Table 4). The

https://doi.org/10.5194/egusphere-2026-5025
Preprint. Discussion started: 16 September 2026

duration of the refilling phase based on the Sentinel-2-derived refilling start and the official GLOF date, shows a decreasing trend from 2016 to 2024, ranging between 119 days in 2017 and 18 days in 2024.

Table 4: Statistics of Sentinel-2-based lake refilling time series. Showing start and end of the refilling phase, the duration of the refilling period, the official GLOF date, the corrected refilling period when using the GLOF date as the end, the total number of available cloud-free Sentinel-2 acquisitions throughout the year and during the refilling period only, the refilling rate based on linear regressions and the trend reliability (R^2).

Year	Refilling start	Refilling end	GLOF date (NVE)	Refilling duration (corrected) [days]	Number of images (total per year) [days]	Number of images (refilling period) [days]
2016	13-Jun	23-Jun	06-Sep	85	15	2
2017	30-Jun	16-Sep	27-Oct	119	18	7
2018	9-May	8-Jul	10-Aug	93	35	19
2019	29-Apr	13-Jul	24-Aug	117	32	10
2020	12-Jun	2-Sep	6-Sep	81	27	9
2021	12-Feb	29-Jun	13-Jul	46	42	10
2022	24-Jun	28-Aug	29-Aug	66	27	4
2023	20-May	14-Jun	22-Jun	33	34	6
2024	14-May	22-May	4-Jun	18	28	3
2025	NaN	NaN	26-Apr	NaN	NaN	NaN

Validation with level logger data and time-lapse camera images

Comparing water area classification results with level logger measurements and time-lapse camera footage from 2023 (Fig. 10) and 2024 (Fig. S3), reveals a generally good agreement in capturing the continuous refilling and drainage of Nedre Demmevatnet. However, the expected underestimation of water area early in the season is evident, for example on 20 May 2023 (Fig. 10), at this stage most of the lake – though clearly visible on the time lapse camera imagery – is still covered with floating ice and consequently classified as ice, snow or shadow in large parts. Later in the season, water classification becomes more accurate (e.g. 14 June 2023, Fig. 10) as most of the lake ice has disappeared.

https://doi.org/10.5194/egusphere-2026-5025
Preprint. Discussion started: 16 September 2026

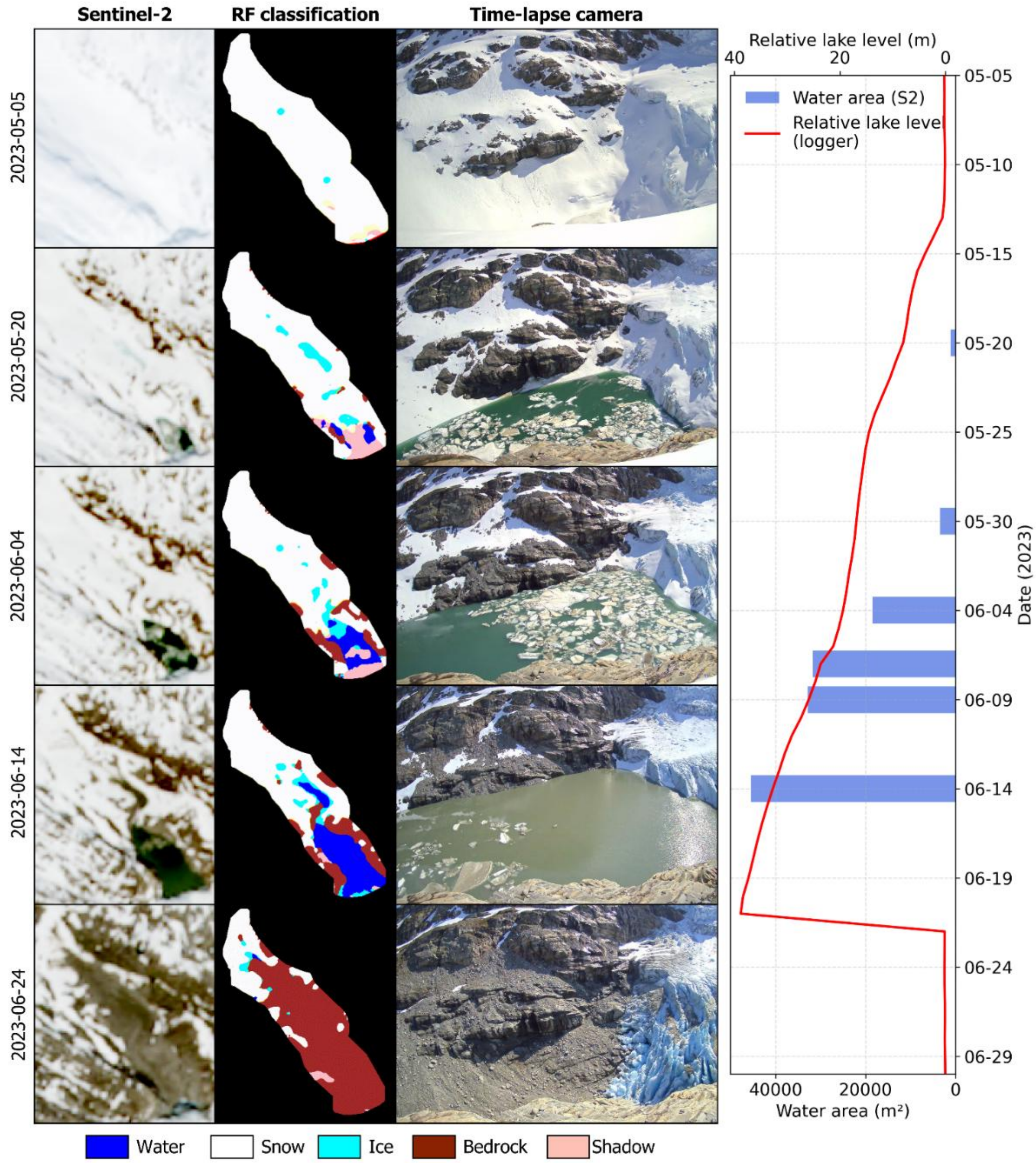

Figure 10: Comparing Sentinel-2 images and RF classifications to time-lapse camera images from the same day and time with level logger measurements (red line) and water area calculations from the Sentinel-2 classification on respective days (blue bars) in 2023.

4.4 Comparison of lake refilling and drainage with weather data

Comparing NORA3 data to AWS data

NORA3 2-m air temperature during summer 2023 correlates well with both AWS Demmevass and AWS Finsevatn air temperature, though a systematic offset of about 2.5°C is evident (Fig. 11; $R^2 = 0.943$ for AWS Finsevatn). Air temperatures were consistently higher at both weather stations than in NORA3, reflecting the median elevation of the NORA3 grid cell

https://doi.org/10.5194/egusphere-2026-5025
Preprint. Discussion started: 16 September 2026

(1469 m a.s.l.), which lies notably higher than either station (AWS Demmevass: 1300 m a.s.l.; AWS Finsevatn: 1210 m a.s.l.). Furthermore, AWS Demmevass captures local meteorological conditions shaped by topography and proximity to the glacier tongue, lake, and mountain slope, whereas NORA3 reflects more general climatic conditions across the wider area.

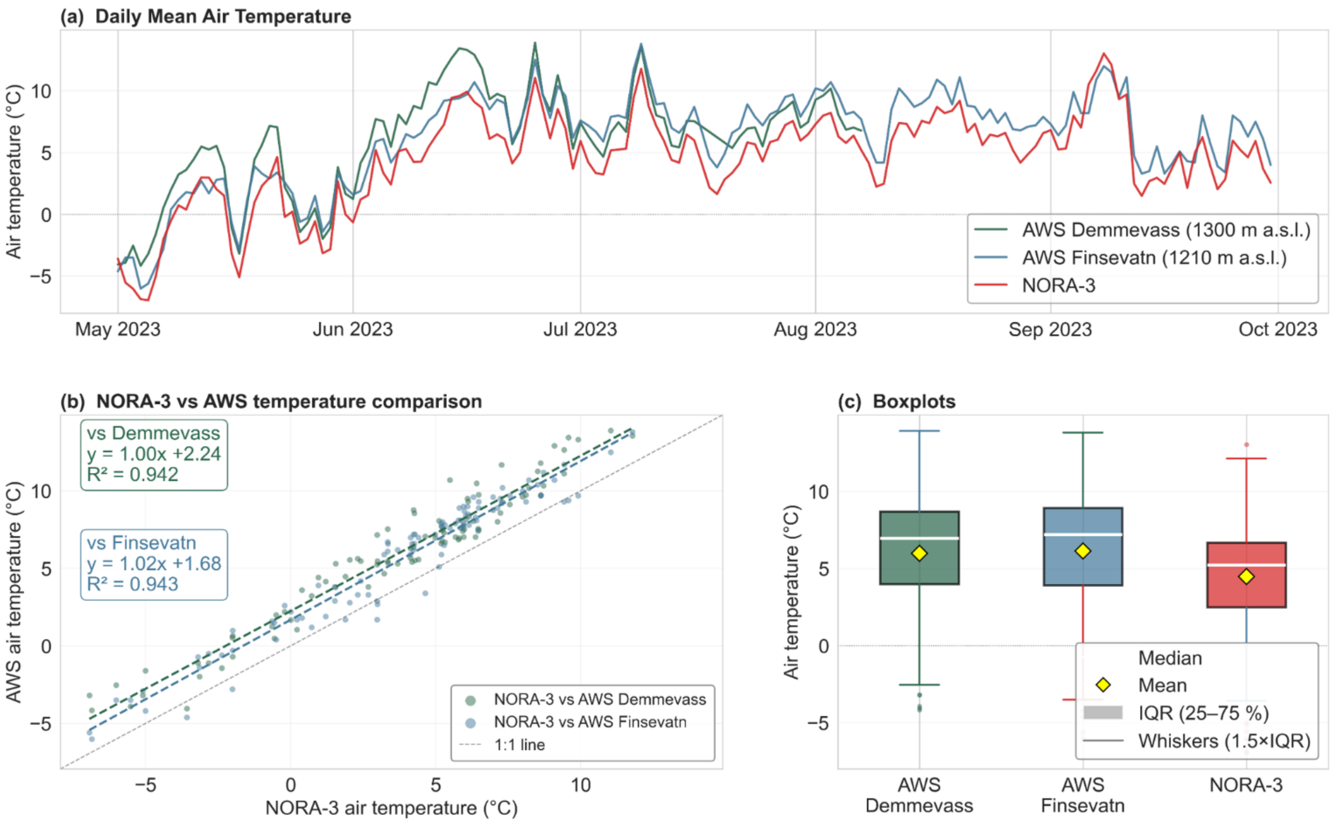

Figure 11: Comparison of daily 2-m air temperature between the closest cell of NORA3 reanalysis data, AWS Demmevass at the Rembesdalskåka glacier tongue, and AWS Finsevatn. (a) Shows air temperature for AWS Demmevass, AWS Finsevatn and for the closest NORA-3 data cell during summer 2023. (b) Scatterplot of NORA-3 data versus each AWS, along with R^2 values, linear regression coefficients, and the 1:1 line. (c) Boxplots for AWS Demmevass, AWS Finsevatn and NORA-3 data for the given period of interest (summer 2023).

Lake refilling and emptying in relation to Positive Degree Day Model and temperature

The timing of lake filling and emptying in relation to melt estimated from the degree-day model, shows that lake filling and emptying seems to have occurred quite consistently after at least 43 melt days for the earlier years until 2022 (Fig. 12). After 2022, however, drainage tended to occur progressively earlier in summer; after only 22 melt days in 2023, and just 4 melt days in 2024. There is a general trend towards earlier drainage observed over the entire period between 2016 and 2025, corresponding to an overall negative glaciological mass balance at Rembesdalskåka since the 1990s (Kjøllmoen et al., 2025) and a retreating glacier front by about 500 m (NVE, 2026a).

https://doi.org/10.5194/egusphere-2026-5025
Preprint. Discussion started: 16 September 2026

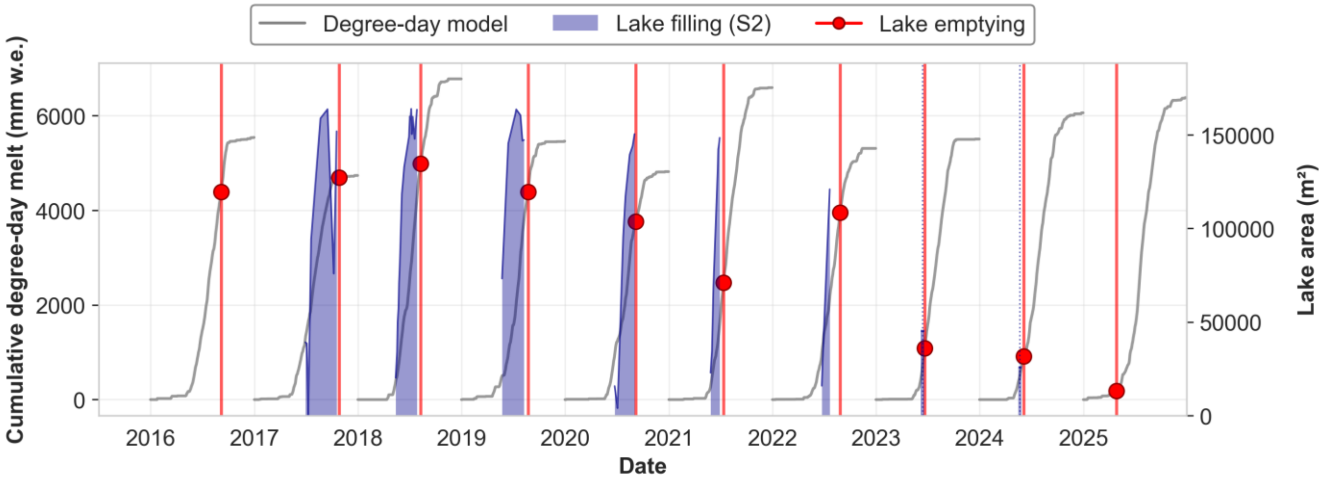

Figure 12: Degree-Day melt and its relationship to lake filling and drainage timing for Nedre Demmevatnet. Degree-day melt was calculated based on a Degree-Day factor of 5.5 mm/C/day for each summer period. Lake filling is derived from the remote sensing analysis (Fig. 9). The timing of lake emptying is based on NVE data (Kjøllmoen et al., 2025; NVE, 2026b).

5 Discussion

5.1 Capabilities and limitations of multi-sensor satellite remote sensing for GLOF monitoring

Addressing RQ1, the reconstruction of GLOF dynamics presented here shows how accurately a multi-sensor satellite remote sensing approach can constrain GLOF timing, volume, level, and sub-seasonal lake evolution at out study area. It also reveals the dominant sources of error, highlighting both the strengths and limitations of our approach. By combining optical Sentinel-2 and radar Sentinel-1 data, we achieved a low temporal uncertainty of ± 2 days for determining lake drainage events across most years. This tight window represents a best-case scenario for GLOF detection with Copernicus data and relies on manual inspection, where all available acquisitions were screened, including partially cloud-covered optical scenes (Fig. S1). In operational or automated detection frameworks, many of these images would likely be excluded, which would reduce detection reliability and temporal resolution. Here, Sentinel-1 imagery worked sufficiently well as a binary tool to confirm the presence or absence of water. This is because calm, specular water surfaces appear dark (low backscatter) in SAR imagery, while the rougher, drained lakebed appears comparatively bright (high backscatter) (Fig. S1). This has also been demonstrated for Messingmalmvatnet, a GLOF site in northern Norway (Andreassen et al., 2025), where Sentinel-1 imagery was used to identify GLOF events. However, in instances where lake drainage happened very early or late in the season while the lake was ice- and snow covered such as demonstrated for 2017 and 2025, satellite-based GLOF detection was not possibly reliable with Copernicus data.

The primary source of error for volume reconstruction of ice-dammed lakes was introduced by the representativeness of the DEM (Table 5), covering the lake's bathymetry as the ice dam position changes over time (Fig. 5). Utilizing the satellite-derived ArcticDEM from 2014 resulted in a systematic volume underestimation of 25.5 % in recent years compared to our field-based 2022 UAV DEM. When subtracting the ArcticDEM from the UAV DEM, we see that the ice dam has retreated by about 50 m, increasing the lake volume due to lost ice volume. This highlights the importance of using the most up-to-date DEM available for GLOF volume reconstructions. A much smaller uncertainty was introduced through the automatically derived Sentinel-2 outlines, which only contributed a volume error of 2.6 - 4.2 % (Table 5).

Table 5: Ranked sources of error in GLOF volume and lake level reconstruction at Nedre Demmevatnet

Source of error (ranked)	Relative volume error [%]	Absolute volume error [M m^3]	Relative lake level error [%]	Absolute lake level error [m]
1. DEM age for lake bathymetry	25.5	0.27	0.01	0.22
2. Sentinel-2 outline accuracy	2.6 - 4.2	0.03 - 0.09	0.02 - 0.05	0.25 – 0.57
3. Gap between pre-GLOF satellite image and GLOF date	1.7/ day	0.03	0.02/ day	0.23 – 0.24

Another important issue, however, remains the availability of completely cloud-free optical images over the lake area, which can create significant time gaps between the latest useful Sentinel-2 image and the actual drainage date, with a maximum of 48 days in 2016 (Fig. 4). Our findings show that for every day of time difference between image acquisition and GLOF, the lake volume is underestimated by a median of 0.03 M m^3, which corresponds to a relative daily underestimation of 1.7 %, representing the largest source of error in volume and lake level reconstructions for some years. Crucially, this error cannot be fixed by using a simple linear correction factor since lake refilling is not always linear as for example shown by the satellite-based refilling time series in 2018 (Fig. 9) or water level logger measurements in 2024 (Fig. S3b), where refilling almost saturates several days prior to drainage. Refilling heavily depends on weather conditions and the state of the ice dam as also shown by Huss et al. (2007) and Veh et al. (2023). To mitigate these time gaps, using in principle daily PlanetScope data helps narrowing the pre-event window, leading to a maximum gap of 13 days (Fig. 4). Even though Sentinel-1 radar offers cloud-penetrating capabilities, it proved insufficient for deriving precise outlines at Nedre Demmevatnet and was therefore not used for volume estimations. The steep alpine terrain causes geometric and topographic distortions, such as layover and shadowing (Fig. 13k), while the smooth surface of wet snow additionally leads to confusion with water (Fig. 13g). Furthermore, a roughened water surface can reduce the specular backscatter signal of water, making it almost indistinguishable from the surrounding landscape (Fig. 13i). Similar issues were also described by Lodigiani et al. (2026) and Wangchuk et al. (2019). However, in other topographic contexts with flatter terrain and larger water body sizes, Sentinel-1 imagery has successfully been used to provide timely and precise lake outlines (Dai et al., 2022; Zhang et al., 2021).

Despite these compounding sources of error, our remote sensing approach yielded overall plausible results that align well with independent field data. This is evident when comparing our UAV- and PlanetScope corrected volume estimates to the official metrics from Statkraft and NVE (Table 6), which are based on surplus inflow into the downstream hydropower reservoir, Rembesdalsvatnet (Kjøllmoen et al., 2025). The values remain within the same order of magnitude across all years, confirming general validity of our method. Statkraft's estimates, however, show a tendency of being lower compared to our

https://doi.org/10.5194/egusphere-2026-5025
Preprint. Discussion started: 16 September 2026

volume estimates, which becomes even more apparent when considering the temporal gap in our data. This discrepancy is logical given the different measurement techniques: downstream reservoir gauges only record the water that has already exited the glacier, missing any floodwater temporarily trapped within subglacial cavities and channels (Huss et al., 2007). This, combined with uncertainties regarding variable background discharge, which may blur the GLOF signal discharge, could explain why Statkraft estimates are lower than ours.

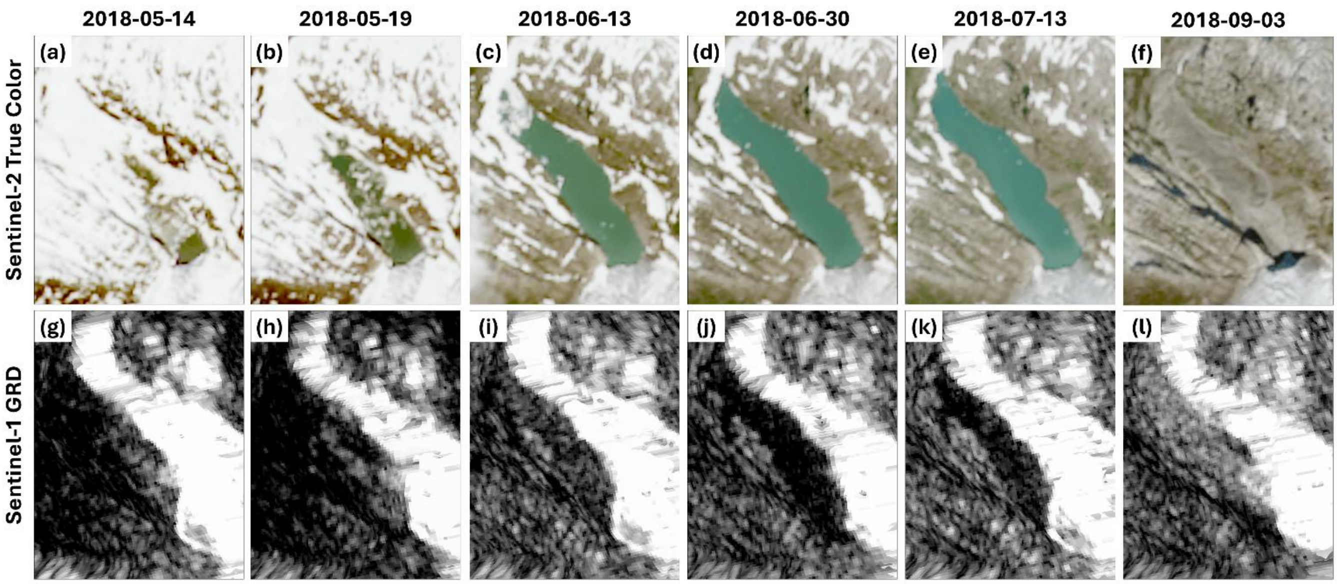

Figure 13: Sub-seasonal comparison of optical and radar imaging capabilities during the 2018 lake refilling phase. (a-f) Sentinel-2 True Color composites tracking the transition from snow-covered to open water. (g-l) Corresponding Sentinel-1 GRD scenes showing geometric distortions (layover and terrain shadowing) caused by steep topography. (g-i) showing the challenge of differentiating the lake boundary from surrounding wet snow and ice early in the season.

Table 6: Comparing PS- and UAV-corrected Sentinel-2 volumes from this study (RS) to volumes estimated by Statkraft as extra inflow to the hydro-power reservoir Rembesdalsvatnet (Kjøllmoen et al., 2025).

Year	Days between S2 img & GLOF	Lake level [m a.s.l.]	Vol. [mio m3] RS	Vol. [mio m3] Statkraft
2016	12	1239	1.99	1.87
2017	9	1236	1.66	1.85
2018	13	1237	1.91	-
2019	9	1238	2.10	1.8
2020	4	1237	2.01	2.3
2021	1	1237	2.11	1.75
2022	0	1238	2.14	2.19
2023	5	1224	0.76	1
2024	1	1236	1.8	1

https://doi.org/10.5194/egusphere-2026-5025
Preprint. Discussion started: 16 September 2026

For assessing sub-seasonal lake refilling with publicly available satellite products, our pixel-based Random Forest model offers a simple framework that robustly tracks water area changes across highly variable conditions, handling transitions from completely snow- and ice-covered landscapes to barren bedrock (Fig. 7). The performance of the classifier can mainly be attributed to the inclusion of the predictors slope and DOY, providing essential topographic and seasonal context, which reduces common misclassification between water, snow, ice and shadow (Abderhalden et al., 2024; Lappe and Andreassen, 2025; Wangchuk and Bolch, 2020). However, as noted in the Sect. 4.3, the high internal accuracy values are likely affected by spatial autocorrelation due to the standard split of training and test data, not effectively representing actual model performance. The real confirmation of the model's reliability comes from its strong agreement with our independent level-logger and time-lapse field data, showing that water area was indeed only depicted within the refilling phases of the lake. The comparison with field data also highlights where the automated workflow falls short: It systematically underestimates water area early in the season when the lake is still fully or partially ice-covered and faces severe challenges detecting water during exceptionally early drainage events, such as in 2025. Furthermore, cloud cover remains a major limitation, leaving substantial data gaps in years like 2016, 2022 or 2024 (Fig. 9), even though we optimized pixel availability using localized cloud probability filters rather than scene-wide thresholds. As noted previously, utilizing Sentinel-1 radar data to fill the data gaps is heavily constrained at Nedre Demmevatnet due to geometric distortions and water misclassification early in the season (Fig. 13). Filling data gaps with PlanetScope data, was also infeasible for our automated approach over a large timescale, as access to the data is limited (see Sect. 3.1.1.) and suffers from variable image quality, which would further complicate scene classification (Abderhalden et al., 2024).

To evaluate the reliability of the NORA3 reanalysis product used to characterize meteorological conditions during lake filling and emptying, we compared the hindcast data against our local AWS Demmevass. This comparison revealed that NORA3 data could only approximate the local weather conditions at Nedre Demmevatnet, because steep terrain and elevation differences introduce high microclimatic variability within the 3x3 km grid cell (Aalto et al., 2017). While 2-m air temperature correlated well with our in-situ meteorological measurements (Fig. 11), there was a systematic cool bias of 2.5°C in the reanalysis data. This discrepancy is primarily driven by the 169 m elevation difference between AWS Demmevass and the average topography of the NORA3 cell (Sect. 4.4). However, this elevation mismatch does not pose a major problem for estimating degree-day melt and lake filling, since a large proportion of the snow- and ice melt contributing to the refilling occurs at higher elevations during spring and early summer. Regarding lake drainage, on the other hand, the degree-day model based on NORA3 data most likely underestimates air temperature and therefore melt on the glacier tongue through which the lake drains. This is because the tongue is situated at a lower altitude than both AWS Demmevass and the average topography of the NORA3 cell. These localized air temperature and melt-rate variations at the glacier tongue would be critical for studying sub- and englacial water input and channel development – processes that ultimately influence drainage timing.

https://doi.org/10.5194/egusphere-2026-5025
Preprint. Discussion started: 16 September 2026

5.2 Towards a transferable GLOF monitoring framework

Addressing RQ2, we synthesized the core operational components of our GLOF monitoring remote sensing framework into a structured implementation checklist (Table 7) to facilitate its potential transferability to GLOF sites that lack in-situ observations. This workflow is designed to scale across different GLOF lakes, provided that specific baseline datasets and adjustments are considered.

Table 7: Implementation framework and checklist for transferring the multi-sensor GLOF monitoring workflow to other glacial lakes, detailing data requirements, processing steps, and local adjustments.

GLOF monitoring step	Required datasets	Core processing steps	Key limitations & local adjustments
1. GLOF timing identification	• S1, S2 imagery archives	• Manual screening of images around suspected GLOF date	• If no regional GLOF inventory exists, the *Seasonal lake refilling* step can be run first to narrow down likely drainage windows.
2. Pre-GLOF volume reconstruction	• Cloud-free pre-event S2 image over lake area • Buffered lake basin polygon • High-resolution DEM of empty lakebed	• Extract lake levels via sub-pixel outline intersection with empty-bed DEM • Calculate volume below lake level	• Requires an updated bathymetric surface. If unavailable, field-based UAV surveys, airborne lidar surveys, commercial stereo-satellite DEMs (e.g. Pléiades), or empirical area-volume equations must be substituted.
3. Seasonal lake refilling	• Complete S2 archive • Regional DEM ideally with full lake (e.g. Copernicus DEM)	• Pixel-based water classification time-series within cloud computing environments GEE/ Python	• Local random forest models require retraining when applied to new regions. Alternatively, global land-cover models can be deployed.
4. Meteorological context	• Gridded reanalysis weather data (e.g. NORA3/ ERA5-Land) • Nearby AWS data (if available)	• Extract daily or sub-daily temperature and precipitation (potentially other variables) spanning the lake refilling and drainage cycle	• Reanalysis data cells for ERA5 (or similar) are large and therefore the data for one grid cell may not be representative of climate/ weather conditions at lake location.

A primary constraint when migrating the proposed workflow to unmonitored study areas is the strict dependency on a high-resolution DEM that accurately captures the empty lakebed topography. For highly dynamic ice-dammed basins, using static, outdated regional DEMs can introduce severe volumetric underestimations due to rapid ice-front retreat and bed erosion (Table 5). If updated field data via UAVs cannot be collected, or commercial VHR stereo imagery (such as Pléiades) or airborne lidar surveys cannot be afforded, this step might be substituted with established empirical volume-area scaling relationships (e.g. Cook and Quincey, 2015). While empirical scaling cannot achieve the high precision of using a bathymetric surface, it still offers an accessible approximation of downstream flood hazards in data-scarce regions.

Furthermore, since our classifier is currently only trained on local data, it cannot simply be applied to other areas without being retrained. Regional differences in water turbidity and chemistry, local rock types, or snowline elevations would otherwise lead to erroneous classifications (Wangchuk and Bolch, 2020). To address this spatial limitation, we tested our automated refilling workflow using the globally standardized Dynamic World land-cover classification (Brown et al., 2022) as an alternative to our locally trained Random Forest model (Fig. S4). While the Dynamic World imagery resulted in slightly lower

https://doi.org/10.5194/egusphere-2026-5025
Preprint. Discussion started: 16 September 2026

data coverage and a higher frequency of false-positive water pixels outside the refilling period, it successfully captured the general seasonal lake-refilling trend. This demonstrates that globally pre-trained models can serve as a functional, low-effort alternative for tracking glacial lake dynamics.

To assess the meteorological context for a glacial lake outside of Norway, NORA3 data would need to be substituted with a regional AWS or a global product like ERA5-Land. However, utilizing ERA5 data introduces much larger regional uncertainty due to its coarser grid cell size of 31 km. Overall, thanks to the primary the use of publicly available data, this monitoring framework should be easily applicable to other glacial lakes worldwide.

5.3 What can we learn about GLOF mechanisms and timing at Nedre Demmevatnet from remote sensing-based monitoring?

Addressing RQ3, our satellite-based monitoring between 2016 and 2025 reveals clear trends in how Nedre Demmevatnet fills and drains, offering important clues about the underlying drainage mechanisms, the structural stability of the ice dam and its response to climate change. First, we see a general trend where GLOFs occur increasingly earlier in the year, shifting forward by 10 days on average over the study period (Fig. 3). This shift directly aligns with the recent thinning of the glacier (Kjøllmoen et al., 2025) as well as with global observations of ice-dammed lakes (Veh et al., 2023), reflecting a systematic response to accelerated atmospheric warming. Complementing this temporal shift, our remote sensing analysis captures a distinct shortening of the seasonal lake-refilling phases (Table 4). It can further be inferred that Nedre Demmevatnet almost never experienced refilling after a GLOF event in this period, strongly suggesting that the subglacial drainage channel remained thermally and hydraulically connected to the glacier's main drainage network following an outburst. This observation is important because it demonstrates that the surrounding ice is no longer thick or dynamic enough to exert the pressure required to deform and closure-seal the subglacial conduit after drainage until winter freeze-up sets in (Huss et al., 2007; Tweed and Russell, 1999). To use our remote sensing analysis for investigating the dominant drainage mechanism at Nedre Demmevatnet, we tested Thorarinsson's (1939) flotation criterion, which assumes that flotation occurs when the water depth reaches roughly 90 % of the ice-dam thickness (H_i). Based on the Arctic DEM and UAV DEM, we identified a critical flotation threshold elevation at about 1239 m a.s.l. in 2014, which declined slightly to about 1233 m a.s.l. in 2022 (Table 8).

Even though the glacier tongue has thinned rapidly over the past decade (Fig. 5), the flotation threshold elevation did not decrease as much as expected because the ice dam retreated into areas of greater ice thickness. As a result, the ice-rim elevation at the ice-lake interface only decreased from 1245 m a.s.l. in 2014 to 1239 m a.s.l. in 2022 (Table 8). When combined with the ice dam retreat, the glacier exposed deeper bedrock bathymetry through increased subglacial erosion, lowering the bottom of the lakebed from 1189 m a.s.l. to 1176 m a.s.l. Consequently, the total ice dam height (H_i) actually increased from 56 m in 2014 to 63 m in 2022, partially offsetting the systemic decline in the absolute flotation elevation. Between 2016 and 2022, the pre-GLOF lake levels derived in this study consistently reached 1236–1239 m a.s.l. (Table 6), closely matching or slightly exceeding the calculated flotation threshold elevations while remaining below the glacier rim elevation. This pattern is consistent with a classic flotation-driven drainage mechanism, in which the lake repeatedly filled to near its maximum

https://doi.org/10.5194/egusphere-2026-5025
Preprint. Discussion started: 16 September 2026

attainable level, before triggering drainage through flotation-induced conduit opening (Tweed and Russell, 1999), providing a possible explanation for the observed drainage behaviour in the years where the flotation threshold was reached.

Table 8: Deriving the flotation threshold [ice dam height * 0.9] based on ArcticDEM and UAV DEM. Ice dam elevation is approximated as the median elevation along the rim at the ice-lake interface.

Year DEM	2014	2022
Lake bottom elevation [m a.s.l.]	1189	1176
Ice dam elevation [m a.s.l.]	1245	1239
Ice dam height (H_i) [m]	56	63
Flotation threshold (H_i * 0.9) [m]	50.4	56.7
Flotation threshold elevation [m a.s.l.]	1239.4	1232.7

The 2023 event, however, represents a marked departure from this record, with drainage initiating at approximately 1224 m a.s.l., more than 10 m below the drainage levels observed during 2016–2022. While this discrepancy could be attributed to measurement uncertainty, as the latest cloud-free satellite image was acquired five days before the GLOF event, it might also indicate a change in drainage mechanism. When comparing our 2023 and 2024 time-lapse camera videos (Fig. 14), it can be confirmed that the lake drained at a lower level in 2023, even though the footage does not allow for an absolute lake level difference quantification.

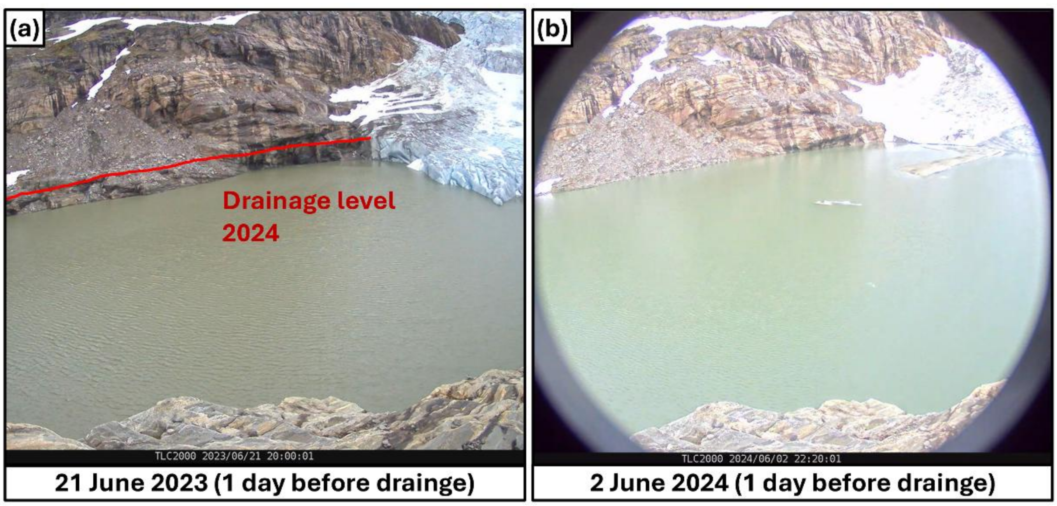

Figure 14: Time-lapse camera footage capturing the day prior to initiation of lake drainage on (a) 21 June 2023 and (b) 2 June 2024. The comparison demonstrates that the lake initiated drainage at a visible lower water level in 2023 than in 2024.

Hence, a possible drainage mechanism in 2023 could be related to subglacial channel development which enables water to exploit and thermally enlarge pre-existing fractures, allowing drainage to occur at lower hydrostatic pressures without

https://doi.org/10.5194/egusphere-2026-5025
Preprint. Discussion started: 16 September 2026

floating the ice dam as well as connecting earlier to the pre-existing subglacial drainage network of the glacier (Jenson et al., 2022; Nye, 1976). This assumption is further supported by the marked shift in earlier outburst timing and degree day melt as seen in Fig. 12, where significantly fewer positive degree days were logged prior to the drainage date after 2022. The observation that the lake reached the flotation threshold again in 2024 under an equally short melt period is more difficult to reconcile with this hypothesis, since degree-day sums alone would suggest limited meltwater generation prior to drainage. However, degree-day estimates only approximate melt driven by air temperature and do not capture other contributions to lake inflow, such as rainfall or radiation-driven melt, which may have compensated for the comparatively low degree-day totals.

Ultimately, since our methodology relies on satellite and aerial surface observations, the proposed subglacial drainage mechanisms remain speculative. Without further direct, high-frequency in-situ observations, such as subglacial water pressure gauges, basal seismometers, or continuous run-off measurements, it is difficult to confirm the exact physical triggers (Carrivick and Tweed, 2016; Tweed and Russell, 1999). In the absence of direct subglacial measurements, a valuable alternative approach to test these hypotheses would be numerical modelling of the glacier's internal drainage system (Kingslake and Ng, 2013; Werder et al., 2013). Simulating the evolution of the subglacial conduit could help clarify whether channel melt enlargement alone is capable of reproducing the observed rapid drainages, or if mechanical initiation via partial ice-dam flotation must be considered a contributing mechanism.

6 Conclusions

This study presents an integrated, multi-sensor reconstruction of the seasonal evolution, drainage timing, and volumetric changes of the ice-dammed lake Nedre Demmevatnet over the period 2016 – 2025. The primary objective of this work was to evaluate the integration of publicly available datasets to establish a detailed, site-specific error budget for tracking a small, highly dynamic glacial lake. By validating satellite observations against in-situ measurements, including a UAV-derived lakebed DEM, water level loggers, and time-lapse imagery, this framework provides a comprehensive benchmark for defining remote sensing capabilities and limitations for glacial lake monitoring. Our findings demonstrate that combining Sentinel-2 imagery with cloud-penetrating Sentinel-1 radar data effectively overcomes high-alpine cloud constraints, narrowing GLOF drainage windows to a temporal ambiguity of ± 2 days. While pixel-based machine-learning with Sentinel-2 data robustly tracks seasonal lake refilling by incorporating slope and temporal variables, the capability of this approach remains impacted by early-season lake ice and severe data gaps in cloudy periods.

Quantifying the error budget reveals that the most critical driver of volumetric uncertainty is the representativeness of the bathymetric DEM, introducing a systematic underestimation of 25.5 % in our study due to a decade of uncaptured glacier retreat and lakebed erosion. The second most significant error source is the temporal gap between the latest available cloud-free satellite acquisition and the actual GLOF date, which introduces a median volume underestimation of 1.7 % per day, that quickly scales up, when the GLOF is preceded by a period of cloudy weather. The geometric uncertainties of the automatically-derived lake outlines remain minor with a relative volume error contribution of 2.6 – 4.2 %. The workflow presented here is

https://doi.org/10.5194/egusphere-2026-5025
Preprint. Discussion started: 16 September 2026

in principle largely transferable to other glacial lakes provided similar data are available (empty bed DEM, satellite overpass frequency, reanalysis data). Evaluating meteorological datasets revealed that while products like NORA3 accurately reflect the general seasonal climate forcing driving lake refilling, steep alpine terrain introduces microclimatic temperature biases that must be carefully considered.

Finally, our integrated, field-validated remote sensing analysis enabled a range of glaciological insights at Nedre Demmevatnet: The lake exhibited a distinct trend toward earlier annual drainage timings – shifting forward by an average of 10 days – and shortened seasonal refilling phases, reflecting a systematic response to accelerated atmospheric warming and related melt rates. Between 2016 and 2022, pre-GLOF lake levels consistently matched or slightly exceeded the calculated flotation threshold elevations, leading to the hypothesis that flotation was at least part of the drainage initiation mechanism at Nedre Demmevatnet. We speculate that the drainage mechanism might have shifted in 2023, possibly to subglacial channel enlargement, as suggested by the notably lower pre-drainage lake level and the shortened melt period indicated by the degree-day analysis. However, these proposed triggering mechanisms remain speculative as they are based on aerial surface observation only. Overall, our study demonstrated that while individual satellite and meteorological datasets possess inherent spatial and temporal limitations in steep alpine terrain, their strategic integration with high-resolution field validation provides a precise and reliable framework for diagnosing drainage dynamics in a rapidly changing ice-dammed lake system.

Data availability

Copernicus data was retrieved via the Google Earth Engine Python API (https://earthengine.google.com/) for the automated parts of the methodology, while Copernicus Browser (https://browser.dataspace.copernicus.eu/) was used for manual image screening. PlanetScope data was downloaded from Planet Labs (https://www.planet.com/) using the free quota of the Education and Research license. The ArcticDEM strip was downloaded through the Polar Geospatial Center (https://www.pgc.umn.edu/data/arcticdem/), while the Norwegian National Elevation Model (NDH-DTM) was accessed through Kartverket's høydedata download portal (https://hoydedata.no/, UUID: 42f30a19-f471-3c86-8635-e87876fd7106). Data from NORA3 was retrieved via https://data.met.no/ and Finse weather station data (SN25830) was retrieved via the Frost API (https://frost.met.no/). The processed DEM from the UAV survey, the level logger and the AWS Demmevass data will be available through the Nasjonal Vitenarkiv as DOIs [provided at the time of publication].

Video supplement

The time-lapse camera videos will be uploaded to Copernicus Publications and be available with DOIs [provided at the time of publication].

Supplement link: The supplementary material is provided in a separate file which is available online.

https://doi.org/10.5194/egusphere-2026-5025
Preprint. Discussion started: 16 September 2026

Author contributions

RL conceptualized the study with supervision from AK, LMA, MC and YG. RL developed the code, analysed and visualised the data with contributions from PE (weather data analysis) and UE (co-registration). Field work was planned and conducted by RL, UE, PE and YG with responsibility for AWS (RL, PE), time-lapse camera (UE), level loggers (RL, UE, PE, YG) and UAV (YG, RL). RL prepared the manuscript with contributions from UE, PE and YG. All co-authors contributed to revisions and read the final manuscript.

Competing interests

The authors declare that they have no conflict of interest.

Acknowledgements

The authors thank Jogscha Abderhalden, Radek Svoboda, Sangita Tomar, Julia Wiel and Sebastian Bø for assisting with field work. We further thank Jens Ådne Rekkedal Haga from the Finse Alpine Research Center (University of Oslo) and Norwegian Trekking Association (DNT) Oslo for logistical support. The field work was mainly financed through the GOTHECA project (https://www.gotheca.com/). This work is a contribution to NVEs R&D project "Karakteristikk, kartlegging og varsling av jøkullaup" and NVE Copernicustjenester.

References

Aalto, J., Riihimäki, H., Meineri, E., Hylander, K., and Luoto, M.: Revealing topoclimatic heterogeneity using meteorological station data, Intl Journal of Climatology, 37, 544–556, https://doi.org/10.1002/joc.5020, 2017.

Abderhalden, J. M., Bly, K. K., Lappe, R., Andreassen, L. M., and Rogozhina, I.: Tracking rapid and slow ice-dammed lake changes through optical satellites and local knowledge: a case study of Tystigbreen in Norway, J. Glaciol., 70, 1–16, https://doi.org/10.1017/jog.2024.13, 2024.

Abriha, D., Srivastava, P. K., and Szabó, S.: Smaller is better? Unduly nice accuracy assessments in roof detection using remote sensing data with machine learning and k-fold cross-validation, Heliyon, 9, e14045, https://doi.org/10.1016/j.heliyon.2023.e14045, 2023.

Aggarwal, A., Jain, S. K., Lohani, A. K., and Jain, N.: Glacial lake outburst flood risk assessment using combined approaches of remote sensing, GIS and dam break modelling, Geomatics, Natural Hazards and Risk, 7, 18–36, https://doi.org/10.1080/19475705.2013.862573, 2016.

Amin, M., Bano, D., Hassan, S. S., Goheer, M. A., Khan, A. A., Khan, M. R., and Hina, S. M.: Mapping and monitoring of glacier lake outburst floods using geospatial modelling approach for Darkut valley, Pakistan, Meteorol Appl, 27, https://doi.org/10.1002/met.1877, 2020.

Andreassen, L. M., Moholdt, G., Kääb, A., Messerli, A., Nagy, T., and Winsvold, S. H.: Monitoring glaciers in mainland Norway and Svalbard using Sentinel, 3/2021, Norwegian Water Resources and Energy Directorate, Oslo, https://publikasjoner.nve.no/rapport/2021/rapport2021_03.pdf (last access: 1 July 2025), 2021.

Andreassen, L. M., Nagy, T., Kjøllmoen, B., and Leigh, J. R.: An inventory of Norway's glaciers and ice-marginal lakes from 2018–19 Sentinel-2 data, J. Glaciol., 68, 1085–1106, https://doi.org/10.1017/jog.2022.20, 2022.

Andreassen, L. M., Blumenrath, S., Engeset, R. V., Kolberg, S. A., Melvold, K., Müller, K., Orthe, N. K., Weber, P., Widforss, A., and Winsvold, S. H.: NVE Copernicustjenester. Sluttrapport for Copernicus aktiviteter i NVE 2022-2024 med anbefalinger, 12/2025, Norges vassdrags- og energidirektorat, Oslo, Norway, https://publikasjoner.nve.no/rapport/2025/rapport2025_12.pdf (last access: 29 June 2026), 2025.

Bazai, N. A., Cui, P., Carling, P. A., Wang, H., Hassan, J., Liu, D., Zhang, G., and Jin, W.: Increasing glacial lake outburst flood hazard in response to surge glaciers in the Karakoram, Earth-Science Reviews, 212, 103432, https://doi.org/10.1016/j.earscirev.2020.103432, 2021.

Bazilova, V. and Kääb, A.: Mapping Area Changes of Glacial Lakes Using Stacks of Optical Satellite Images, Remote Sensing, 14, 5973, https://doi.org/10.3390/rs14235973, 2022.

Bengtsson, L., Andrae, U., Aspelien, T., Batrak, Y., Calvo, J., De Rooy, W., Gleeson, E., Hansen-Sass, B., Homleid, M., Hortal, M., Ivarsson, K.-I., Lenderink, G., Niemelä, S., Nielsen, K. P., Onvlee, J., Rontu, L., Samuelsson, P., Muñoz, D. S., Subias, A., Tijm, S., Toll, V., Yang, X., and Køltzow, M. Ø.: The HARMONIE–AROME Model Configuration in the ALADIN–HIRLAM NWP System, Monthly Weather Review, 145, 1919–1935, https://doi.org/10.1175/MWR-D-16-0417.1, 2017.

Benn, D. and Evans, D. J. A.: Glaciers and Glaciation, 2nd ed., Routledge, https://doi.org/10.4324/9780203785010, 2014.

Bolch, T., Buchroithner, M. F., Peters, J., Baessler, M., and Bajracharya, S.: Identification of glacier motion and potentially dangerous glacial lakes in the Mt. Everest region/Nepal using spaceborne imagery, Nat. Hazards Earth Syst. Sci., 8, 1329–1340, https://doi.org/10.5194/nhess-8-1329-2008, 2008.

Braithwaite, R. J. and Raper, S. C. B.: Glaciological conditions in seven contrasting regions estimated with the degree-day model, Ann. Glaciol., 46, 297–302, https://doi.org/10.3189/172756407782871206, 2007.

Brown, C. F., Brumby, S. P., Guzder-Williams, B., Birch, T., Hyde, S. B., Mazzariello, J., Czerwinski, W., Pasquarella, V. J., Haertel, R., Ilyushchenko, S., Schwehr, K., Weisse, M., Stolle, F., Hanson, C., Guinan, O., Moore, R., and Tait, A. M.: Dynamic World, Near real-time global 10 m land use land cover mapping, Sci Data, 9, 251, https://doi.org/10.1038/s41597-022-01307-4, 2022.

Carrivick, J. L. and Tweed, F. S.: A global assessment of the societal impacts of glacier outburst floods, Global and Planetary Change, 144, 1–16, https://doi.org/10.1016/j.gloplacha.2016.07.001, 2016.

Carrivick, J. L., Tweed, F. S., Ng, F., Quincey, D. J., Mallalieu, J., Ingeman-Nielsen, T., Mikkelsen, A. B., Palmer, S. J., Yde, J. C., Homer, R., Russell, A. J., and Hubbard, A.: Ice-Dammed Lake Drainage Evolution at Russell Glacier, West Greenland, Front. Earth Sci., 5, 100, https://doi.org/10.3389/feart.2017.00100, 2017.

Cook, S. J. and Quincey, D. J.: Estimating the volume of Alpine glacial lakes, Earth Surf. Dynam., 3, 559–575, https://doi.org/10.5194/esurf-3-559-2015, 2015.

https://doi.org/10.5194/egusphere-2026-5025
Preprint. Discussion started: 16 September 2026

Dai, K., Wen, N., Fan, X., Deng, J., Zhang, L., Liang, R., Liu, J., and Xu, Q.: Seasonal Changes of Glacier Lakes in Tibetan Plateau Revealed by Multipolarization SAR Data, IEEE Geosci. Remote Sensing Lett., 19, 1–5, https://doi.org/10.1109/LGRS.2021.3131717, 2022.

Drusch, M., Del Bello, U., Carlier, S., Colin, O., Fernandez, V., Gascon, F., Hoersch, B., Isola, C., Laberinti, P., Martimort, P., Meygret, A., Spoto, F., Sy, O., Marchese, F., and Bargellini, P.: Sentinel-2: ESA's Optical High-Resolution Mission for GMES Operational Services, Remote Sensing of Environment, 120, 25–36, https://doi.org/10.1016/j.rse.2011.11.026, 2012.

Elvehøy, H., Kohler, J., Engeset, R., and Andreassen, L. M.: Jøkullaup fra Demmevatn, 17, Norges Vassdrags- og Energiverk, Oslo, Norway, http://publikasjoner.nve.no/rapport/1997/rapport1997_17.pdf (last access: 23 June 2026), 1997.

Elvehøy, H., Engeset, R. V., Andreassen, L. M., Kohler, J., Gjessing, Y., and Björnsson, H.: Assessment of possible jøkulhlaups from Lake Demmevatn in Norway, The Extremes of the Extremes: Extraordinary floods., 271, 31–36, 2002.

Emmer, A., Allen, S. K., Carey, M., Frey, H., Huggel, C., Korup, O., Mergili, M., Sattar, A., Veh, G., Chen, T. Y., Cook, S. J., Correas-Gonzalez, M., Das, S., Diaz Moreno, A., Drenkhan, F., Fischer, M., Immerzeel, W. W., Izagirre, E., Joshi, R. C., Kougkoulos, I., Kuyakanon Knapp, R., Li, D., Majeed, U., Matti, S., Moulton, H., Nick, F., Piroton, V., Rashid, I., Reza, M., Ribeiro de Figueiredo, A., Riveros, C., Shrestha, F., Shrestha, M., Steiner, J., Walker-Crawford, N., Wood, J. L., and Yde, J. C.: Progress and challenges in glacial lake outburst flood research (2017–2021): a research community perspective, Other Hazards (e.g., Glacial and Snow Hazards, Karst, Wildfires Hazards, and Medical Geo-Hazards), https://doi.org/10.5194/nhess-2022-143, 2022.

Engeset, R. V., Schuler, T. V., and Jackson, M.: Analysis of the first jökulhlaup at Blåmannsisen, northern Norway, and implications for future events, Ann. Glaciol., 42, 35–41, https://doi.org/10.3189/172756405781812600, 2005.

EO Research: https://medium.com/sentinel-hub/cloud-masks-at-your-service-6e5b2cb2ce8a, https://medium.com/sentinel-hub/cloud-masks-at-your-service-6e5b2cb2ce8a (last access: 7 April 2026), 2020., 2020.

ESA: https://www.esa.int/Applications/Observing_the_Earth/Copernicus/Sentinel-1/Watch_live_Vega-C_to_launch_Sentinel-1C, https://www.esa.int/Applications/Observing_the_Earth/Copernicus/Sentinel-1/Watch_live_Vega-C_to_launch_Sentinel-1C (last access: 25 May 2026), 2024., 2024.

ESA: Sentinel-1 mission, https://sentiwiki.copernicus.eu/web/s1-mission, last access: 5 April 2024a, 2025., 2025.

ESA: Sentinel-2, , sentiwiki, 2025b.

ESA: The Sentinel missions, , Applications, 2026.

ESA and Airbus: Copernicus DEM, https://doi.org/10.5270/ESA-c5d3d65, 2022.

Feyisa, G. L., Meilby, H., Fensholt, R., and Proud, S. R.: Automated Water Extraction Index: A new technique for surface water mapping using Landsat imagery, Remote Sensing of Environment, 140, 23–35, https://doi.org/10.1016/j.rse.2013.08.029, 2014.

Furevik, B. R. and Haakenstad, H.: NORA3 atmosphere hindcast data. Norwegian Meterological Institute, https://data.met.no/dataset/64636e8c-c486-4496-bdda-89687e1d8f97 (last access: 19 August 2026), 2025.

Gascon, F., Bouzinac, C., Thépaut, O., Jung, M., Francesconi, B., Louis, J., Lonjou, V., Lafrance, B., Massera, S., Gaudel-Vacaresse, A., Languille, F., Alhammoud, B., Viallefont, F., Pflug, B., Bieniarz, J., Clerc, S., Pessiot, L., Trémas, T., Cadau,

https://doi.org/10.5194/egusphere-2026-5025
Preprint. Discussion started: 16 September 2026

E., De Bonis, R., Isola, C., Martimort, P., and Fernandez, V.: Copernicus Sentinel-2A Calibration and Products Validation Status, Remote Sensing, 9, 584, https://doi.org/10.3390/rs9060584, 2017.

GEE: Sentinel-2: Cloud Probability, https://developers.google.com/earth-engine/datasets/catalog/COPERNICUS_S2_CLOUD_PROBABILITY?hl=en, 2025.

Glasbey, C. A.: An Analysis of Histogram-Based Thresholding Algorithms, CVGIP: Graphical Models and Image Processing, 55, 532–537, https://doi.org/10.1006/cgip.1993.1040, 1993.

Gorelick, N., Hancher, M., Dixon, M., Ilyushchenko, S., Thau, D., and Moore, R.: Google Earth Engine: Planetary-scale geospatial analysis for everyone, Remote Sensing of Environment, 202, 18–27, https://doi.org/10.1016/j.rse.2017.06.031, 2017.

Haakenstad, H. and Breivik, Ø.: NORA3. Part II: Precipitation and Temperature Statistics in Complex Terrain Modeled with a Nonhydrostatic Model, Journal of Applied Meteorology and Climatology, 61, 1549–1572, https://doi.org/10.1175/JAMC-D-22-0005.1, 2022.

Haakenstad, H., Breivik, Ø., Furevik, B. R., Reistad, M., Bohlinger, P., and Aarnes, O. J.: NORA3: A Nonhydrostatic High-Resolution Hindcast of the North Sea, the Norwegian Sea, and the Barents Sea, Journal of Applied Meteorology and Climatology, 60, 1443–1464, https://doi.org/10.1175/JAMC-D-21-0029.1, 2021.

Harrison, S., Kargel, J. S., Huggel, C., Reynolds, J., Shugar, D. H., Betts, R. A., Emmer, A., Glasser, N., Haritashya, U. K., Klimeš, J., Reinhardt, L., Schaub, Y., Wiltshire, A., Regmi, D., and Vilímek, V.: Climate change and the global pattern of moraine-dammed glacial lake outburst floods, The Cryosphere, 12, 1195–1209, https://doi.org/10.5194/tc-12-1195-2018, 2018.

Huggel, C., Haeberli, W., Kääb, A., Bieri, D., and Richardson, S.: An assessment procedure for glacial hazards in the Swiss Alps, Can. Geotech. J., 41, 1068–1083, https://doi.org/10.1139/t04-053, 2004.

Huss, M., Bauder, A., Werder, M., Funk, M., and Hock, R.: Glacier-dammed lake outburst events of Gornersee, Switzerland, J. Glaciol., 53, 189–200, https://doi.org/10.3189/172756507782202784, 2007.

Jackson, M. and Ragulina, G.: Inventory of glacier-related hazardous events in Norway, 83, Norwegian Water Resources and Energy Directorate, Oslo, https://publikasjoner.nve.no/rapport/2014/rapport2014_83.pdf, 2014.

Jenson, A., Amundson, J. M., Kingslake, J., and Hood, E.: Long-period variability in ice-dammed glacier outburst floods due to evolving catchment geometry, The Cryosphere, 16, 333–347, https://doi.org/10.5194/tc-16-333-2022, 2022.

Kääb, A., Winsvold, S., Altena, B., Nuth, C., Nagler, T., and Wuite, J.: Glacier Remote Sensing Using Sentinel-2. Part I: Radiometric and Geometric Performance, and Application to Ice Velocity, Remote Sensing, 8, 598, https://doi.org/10.3390/rs8070598, 2016.

Kartverket: Nasjonal detaljert høydemodell, https://www.kartverket.no/en/geodataarbeid/nasjonal-detaljert-hoydemodell/status-hoydemodell (last access: 13 April 2026), 2025.

Keshri, A. K., Shukla, A., and Gupta, R. P.: ASTER ratio indices for supraglacial terrain mapping, International Journal of Remote Sensing, 30, 519–524, https://doi.org/10.1080/01431160802385459, 2009.

Kingslake, J. and Ng, F.: Modelling the coupling of flood discharge with glacier flow during jökulhlaups, Ann. Glaciol., 54, 25–31, https://doi.org/10.3189/2013AoG63A331, 2013.

Kjøllmoen, B., Elvehøy, H., and Andreassen, L. M.: Glaciological investigations in Norway 2022, Norwegian Water Resources and Energy Directorate, Oslo, https://publikasjoner.nve.no/rapport/2022/rapport2022_27.pdf (last access: 20 May 2026), 2022.

Kjøllmoen, B., Andreassen, L. M., and Hallgeir Elvehøy: Glaciological investigations in Norway 2024, https://doi.org/10.58059/2XVM-1X48, 2025.

Lappe, R. and Andreassen, L. M.: Updating Norways glacial lake inventory - an automated workflow using Sentinel-1 & 2 data and machine learning, https://doi.org/10.5194/egusphere-egu25-17460, 2025., 2025.

Lappe, R. and Andreassen, L. M.: Updating Norway's glacial lake extents in 2023–2024 using Sentinel-1 & Sentinel-2 data and machine learning, J. Glaciol., 72, e16, https://doi.org/10.1017/jog.2026.10131, 2026.

Laumann, T. and Reeh, N.: Sensitivity to climate change of the mass balance of glaciers in southern Norway, J. Glaciol., 39, 656–665, https://doi.org/10.3189/S0022143000016555, 1993.

Liestøl, O.: Glacier Dammed Lakes in Norway, Norsk Geografisk Tidsskrift - Norwegian Journal of Geography, 15, 122–149, https://doi.org/10.1080/00291955608542772, 1956.

Lodigiani, M., Karbou, F., Doridant, J.-B., Demolis, B., Nicora, M., James, G., Adrien, P., Bonnetain, V., Gindraux, S., Mondardini, L., Perret, P., and Troilo, F.: Remote sensing for glacial lakes detection: a multi-sensor approach for mapping and monitoring lakes in Western Alps, Int. Arch. Photogramm. Remote Sens. Spatial Inf. Sci., XLVIII-M-11–2026, 23–29, https://doi.org/10.5194/isprs-archives-XLVIII-M-11-2026-23-2026, 2026.

McFeeters, S. K.: The use of the Normalized Difference Water Index (NDWI) in the delineation of open water features, International Journal of Remote Sensing, 17, 1425–1432, https://doi.org/10.1080/01431169608948714, 1996.

MET Norway: Finsevatn weather station (SN25839), observational data, https://seklima.met.no/ (last access: 19 August 2026), 2025.

Montero, D., Aybar, C., Mahecha, M. D., Martinuzzi, F., Söchting, M., and Wieneke, S.: A standardized catalogue of spectral indices to advance the use of remote sensing in Earth system research, Sci Data, 10, 197, https://doi.org/10.1038/s41597-023-02096-0, 2023.

Müller, M., Homleid, M., Ivarsson, K.-I., Køltzow, M. A. Ø., Lindskog, M., Midtbø, K. H., Andrae, U., Aspelien, T., Berggren, L., Bjørge, D., Dahlgren, P., Kristiansen, J., Randriamampianina, R., Ridal, M., and Vignes, O.: AROME-MetCoOp: A Nordic Convective-Scale Operational Weather Prediction Model, Weather and Forecasting, 32, 609–627, https://doi.org/10.1175/WAF-D-16-0099.1, 2017.

Nagy, T. and Andreassen, L. M.: Glacier lake mapping with Sentinel-2 imagery in Norway, 40–2019, Norwegian Water Resources and Energy Directorate, Oslo, Norway, chrome-extension://efaidnbmnnnibpcajpcglclefindmkaj/https://publikasjoner.nve.no/rapport/2019/rapport2019_40.pdf (last access: 15 November 2024a), 2019.

Nagy, T. and Andreassen, L. M.: Glacier surface velocity mapping with Sentinel-2 imagery in Norway, NVE Rapport, 37/2019, NVE, Oslo, Norway, http://publikasjoner.nve.no/rapport/2019/rapport2019_37.pdf (last access: 13 May 2022b), 2019.

Narama, C., Daiyrov, M., Duishonakunov, M., Tadono, T., Sato, H., Kääb, A., Ukita, J., and Abdrakhmatov, K.: Large drainages from short-lived glacial lakes in the Teskey Range, Tien Shan Mountains, Central Asia, Nat. Hazards Earth Syst. Sci., 18, 983–995, https://doi.org/10.5194/nhess-18-983-2018, 2018.

https://doi.org/10.5194/egusphere-2026-5025
Preprint. Discussion started: 16 September 2026

Ng, H.-F., Jargalsaikhan, D., Tsai, H.-C., and Lin, C.-Y.: An improved method for image thresholding based on the valley-emphasis method, in: 2013 Asia-Pacific Signal and Information Processing Association Annual Summit and Conference, 2013 Asia-Pacific Signal and Information Processing Association Annual Summit and Conference (APSIPA), 1–4, https://doi.org/10.1109/APSIPA.2013.6694261, 2013.

Nie, Y., Liu, Q., and Liu, S.: Glacial Lake Expansion in the Central Himalayas by Landsat Images, 1990–2010, PLoS ONE, 8, e83973, https://doi.org/10.1371/journal.pone.0083973, 2013.

Nieto, L., Schwalbert, R., Prasad, P. V. V., Olson, B. J. S. C., and Ciampitti, I. A.: An integrated approach of field, weather, and satellite data for monitoring maize phenology, Sci Rep, 11, 15711, https://doi.org/10.1038/s41598-021-95253-7, 2021.

Nuth, C. and Kääb, A.: Co-registration and bias corrections of satellite elevation data sets for quantifying glacier thickness change, The Cryosphere, 5, 271–290, https://doi.org/10.5194/tc-5-271-2011, 2011.

NVE: Climate indicator products, http://glacier.nve.no/viewer/CI/ (last access: 9 June 2026a), 2026.

NVE: Glacier lake outburst floods, https://glacier.nve.no/Glacier/viewer/GLOF/enno/ (last access: 25 June 2026b), 2026.

Nye, J. F.: Water Flow in Glaciers: Jökulhlaups, Tunnels and Veins, J. Glaciol., 17, 181–207, https://doi.org/10.3189/S002214300001354X, 1976.

Over, JS. R., Ritchie, A. C., Kranenburg, C. J., Brown, J. A., Duscombe, D. D., Noble, T., Sherwood, C. R., Warrick, J., and Wernette, P. A.: Processing Coastal Imagery With Agisoft Metashape Professional Edition, Version 1.6—Structure From Motion Workflow Documentation, Open-File Report, U.S. Geological Survey, Reston, VA, https://doi.org/https://doi.org/10.3133/ofr20211039, 2021.

Planet: PlanetScope Product Specifications, Planet/ ESA, online, https://planet.widen.net/s/vswqcrm9zw/planet-userdocumentation-psscene-productspec (last access: 26 May 2025), 2023.

Porter, C., Howat, I., Noh, M.-J., Husby, E., Khuvis, S., Danish, E., Tomko, K., Gardiner, J., Negrete, A., Yadav, B., Klassen, J., Kelleher, C., Cloutier, M., Bakker, J., Enos, J., Arnold, G., Bauer, G., Morin, P., and Polar Geospatial Center: ArcticDEM - Strips, Version 4.1 (1.4), https://doi.org/10.7910/DVN/C98DVS, 2022.

QGIS project: Georeferencer (3.44), https://docs.qgis.org/3.44/en/docs/user_manual/managing_data_source/georeferencer.html (last access: 30 March 2026), 2026.

Račič, M., Oštir, K., Zupanc, A., and Čehovin Zajc, L.: Multi-Year Time Series Transfer Learning: Application of Early Crop Classification, Remote Sensing, 16, 270, https://doi.org/10.3390/rs16020270, 2024.

Rawlins, L. D., Watson, C. S., Bhambri, R., Khadka, N., and Chand, M. B.: Glacial Lake Observatory (GLO): Annual dataset of glacial lakes in Nepal and transboundary catchments (2017–2024), https://doi.org/10.5194/essd-2025-751, 12 January 2026., 2026.

Rick, B., McGrath, D., McCoy, S. W., and Armstrong, W. H.: Unchanged frequency and decreasing magnitude of outbursts from ice-dammed lakes in Alaska, Nat Commun, 14, 6138, https://doi.org/10.1038/s41467-023-41794-6, 2023.

Riggs, G. A., Hall, D. K., and Salomonson, V. V.: A snow index for the Landsat Thematic Mapper and Moderate Resolution Imaging Spectroradiometer, in: Proceedings of IGARSS '94 - 1994 IEEE International Geoscience and Remote Sensing

https://doi.org/10.5194/egusphere-2026-5025
Preprint. Discussion started: 16 September 2026

Symposium, IGARSS '94 - 1994 IEEE International Geoscience and Remote Sensing Symposium, 1942–1944, https://doi.org/10.1109/IGARSS.1994.399618, 1994.

Rouse, J. W., Jr., Haas, R. H., Schell, J. A., and Deering, D. W.: Monitoring vegetation systems in the Great Plains with ERTS, Goddard Space Flight Center 3d ERTS-1 Symp, 1974.

Seity, Y., Brousseau, P., Malardel, S., Hello, G., Bénard, P., Bouttier, F., Lac, C., and Masson, V.: The AROME-France Convective-Scale Operational Model, Monthly Weather Review, 139, 976–991, https://doi.org/10.1175/2010MWR3425.1, 2011.

Sentinel-Hub: EO Browser, https://apps.sentinel-hub.com/eo-browser/, 2025.

Shugar, D. H., Burr, A., Haritashya, U. K., Kargel, J. S., Watson, C. S., Kennedy, M. C., Bevington, A. R., Betts, R. A., Harrison, S., and Strattman, K.: Rapid worldwide growth of glacial lakes since 1990, Nat. Clim. Chang., 10, 939–945, https://doi.org/10.1038/s41558-020-0855-4, 2020.

Simoes, R., Camara, G., Queiroz, G., Souza, F., Andrade, P. R., Santos, L., Carvalho, A., and Ferreira, K.: Satellite Image Time Series Analysis for Big Earth Observation Data, Remote Sensing, 13, 2428, https://doi.org/10.3390/rs13132428, 2021.

Strozzi, T., Wiesmann, A., Kääb, A., Joshi, S., and Mool, P.: Glacial lake mapping with very high resolution satellite SAR data, Nat. Hazards Earth Syst. Sci., 12, 2487–2498, https://doi.org/10.5194/nhess-12-2487-2012, 2012.

Taylor, C., Robinson, T. R., Dunning, S., Rachel Carr, J., and Westoby, M.: Glacial lake outburst floods threaten millions globally, Nat Commun, 14, 487, https://doi.org/10.1038/s41467-023-36033-x, 2023.

Thorarinsson, S.: Chapter IX. The ice dammed lakes of Iceland with particular reference to their values as indicators of glacier oscillations, Geografiska Annaler, 21, 216–242, https://doi.org/10.1080/20014422.1939.11880679, 1939.

Tom, M., Odermatt, D., David, C. H., Cerbelaud, A., Wade, J., and Frey, H.: Monitoring earth's glacial lakes from space with machine learning, Science of Remote Sensing, 12, 100277, https://doi.org/10.1016/j.srs.2025.100277, 2025.

Torres, R., Snoeij, P., Geudtner, D., Bibby, D., Davidson, M., Attema, E., Potin, P., Rommen, B., Floury, N., Brown, M., Traver, I. N., Deghaye, P., Duesmann, B., Rosich, B., Miranda, N., Bruno, C., L'Abbate, M., Croci, R., Pietropaolo, A., Huchler, M., and Rostan, F.: GMES Sentinel-1 mission, Remote Sensing of Environment, 120, 9–24, https://doi.org/10.1016/j.rse.2011.05.028, 2012.

Tveito, O. E.: Norwegian standard climate normals 1991-2020 - the methodological approach, 05, Norwegian Meterological Institute, https://www.met.no/publikasjoner/met-report/met-report-2021/_/attachment/download/31bb0160-d8cf-4a2b-9646-4df6f5904059:3ac4fec6cf3fb7919aefe42db2b63ad8e8b9e6a6/METreport%2005_2021_New_Norwegian_standard_climate_normals_1991_2020-signert.pdf (last access: 13 August 2026), 2021.

Tweed, F. S. and Russell, A. J.: Controls on the formation and sudden drainage of glacier-impounded lakes: implications for jökulhlaup characteristics, Progress in Physical Geography: Earth and Environment, 23, 79–110, https://doi.org/10.1177/030913339902300104, 1999.

Van Der Walt, S., Schönberger, J. L., Nunez-Iglesias, J., Boulogne, F., Warner, J. D., Yager, N., Gouillart, E., and Yu, T.: scikit-image: image processing in Python, PeerJ, 2, e453, https://doi.org/10.7717/peerj.453, 2014.

Veh, G., Korup, O., Von Specht, S., Roessner, S., and Walz, A.: Unchanged frequency of moraine-dammed glacial lake outburst floods in the Himalaya, Nat. Clim. Chang., 9, 379–383, https://doi.org/10.1038/s41558-019-0437-5, 2019.

https://doi.org/10.5194/egusphere-2026-5025
Preprint. Discussion started: 16 September 2026

Veh, G., Lützow, N., Tamm, J., Luna, L. V., Hugonnet, R., Vogel, K., Geertsema, M., Clague, J. J., and Korup, O.: Less extreme and earlier outbursts of ice-dammed lakes since 1900, Nature, 614, 701–707, https://doi.org/10.1038/s41586-022-05642-9, 2023.

Veh, G., Wang, B. G., Zirzow, A., Schmidt, C., Lützow, N., Steppat, F., Zhang, G., Vogel, K., Geertsema, M., Clague, J. J., and Korup, O.: Progressively smaller glacier lake outburst floods despite worldwide growth in lake area, Nat Water, https://doi.org/10.1038/s44221-025-00388-w, 2025.

Wang, W., Xiang, Y., Gao, Y., Lu, A., and Yao, T.: Rapid expansion of glacial lakes caused by climate and glacier retreat in the Central Himalayas: RAPID EXPANSION OF GLACIAL LAKES IN THE CENTRAL HIMALAYAS, Hydrol. Process., 29, 859–874, https://doi.org/10.1002/hyp.10199, 2015.

Wangchuk, S. and Bolch, T.: Mapping of glacial lakes using Sentinel-1 and Sentinel-2 data and a random forest classifier: Strengths and challenges, Science of Remote Sensing, 2, 100008, https://doi.org/10.1016/j.srs.2020.100008, 2020.

Wangchuk, S., Bolch, T., and Zawadzki, J.: Towards automated mapping and monitoring of potentially dangerous glacial lakes in Bhutan Himalaya using Sentinel-1 Synthetic Aperture Radar data, International Journal of Remote Sensing, 40, 4642–4667, https://doi.org/10.1080/01431161.2019.1569789, 2019.

Wangchuk, S., Bolch, T., and Robson, B. A.: Monitoring glacial lake outburst flood susceptibility using Sentinel-1 SAR data, Google Earth Engine, and persistent scatterer interferometry, Remote Sensing of Environment, 271, 112910, https://doi.org/10.1016/j.rse.2022.112910, 2022.

Werder, M. A., Hewitt, I. J., Schoof, C. G., and Flowers, G. E.: Modeling channelized and distributed subglacial drainage in two dimensions: A 2-D SUBGLACIAL DRAINAGE SYSTEM MODEL, J. Geophys. Res. Earth Surf., 118, 2140–2158, https://doi.org/10.1002/jgrf.20146, 2013.

xDEM contributors: xDEM (v0.2.0), https://doi.org/10.5281/ZENODO.4809697, 2026.

Yuan, Y. and Lin, L.: Self-Supervised Pre-Training of Transformers for Satellite Image Time Series Classification, https://doi.org/10.36227/techrxiv.13025039.v3, 2 November 2020., 2020.

Zhang, B., Liu, G., Zhang, R., Fu, Y., Liu, Q., Cai, J., Wang, X., and Li, Z.: Monitoring Dynamic Evolution of the Glacial Lakes by Using Time Series of Sentinel-1A SAR Images, Remote Sensing, 13, 1313, https://doi.org/10.3390/rs13071313, 2021.

Zhang, G., Yao, T., Xie, H., Wang, W., and Yang, W.: An inventory of glacial lakes in the Third Pole region and their changes in response to global warming, Global and Planetary Change, 131, 148–157, https://doi.org/10.1016/j.gloplacha.2015.05.013, 2015.

Zhang, G., Carrivick, J. L., Emmer, A., Shugar, D. H., Veh, G., Wang, X., Labedz, C., Mergili, M., Mölg, N., Huss, M., Allen, S., Sugiyama, S., and Lützow, N.: Characteristics and changes of glacial lakes and outburst floods, Nat Rev Earth Environ, 5, 447–462, https://doi.org/10.1038/s43017-024-00554-w, 2024.

Zhang, G., Zheng, G., Khadka, N., Rinzin, S., Tang, Q., Wang, X., Li, J., and Carrivick, J. L.: Challenges in predicting glacial lake outburst floods and suggested pathways forward, The Innovation, 7, 101349, https://doi.org/10.1016/j.xinn.2026.101349, 2026.

https://doi.org/10.5194/egusphere-2026-5025
Preprint. Discussion started: 16 September 2026

Zheng, G., Allen, S. K., Bao, A., Ballesteros-Cánovas, J. A., Huss, M., Zhang, G., Li, J., Yuan, Y., Jiang, L., Yu, T., Chen, W., and Stoffel, M.: Increasing risk of glacial lake outburst floods from future Third Pole deglaciation, Nat. Clim. Chang., 11, 411–417, https://doi.org/10.1038/s41558-021-01028-3, 2021.